Acta Geotechnica
https://doi.org/10.1007/s11440-022-01634-1

RESEARCH PAPER

Creep characteristics of calcareous coral sand in the South China Sea

Jianhong Ye[1] · Yeernaer Haiyilati[2,1] · Meng Cao[2,1] · Dianjun Zuo[3] · Xiuwei Chai[4]

Received: 25 October 2020 / Accepted: 28 June 2022
© The Author(s), under exclusive licence to Springer-Verlag GmbH Germany, part of Springer Nature 2022

Abstract
In recent years, a series of lands have been built or enlarged on the top of some natural coral reefs by the means of reclamation in the South China Sea (SCS). The reclamation material used is the calcareous coral sand extracted from nearby lagoons. As a kind of special geotechnical material, its mechanical characteristics are different from that of conventional terrestrial soil. It is of great significance to study the time-dependent creep characteristics of the calcareous coral sand for evaluating the post-construction settlement of some important structures built on these reclaimed lands. In this study, a series of drained triaxial tests are conducted to study the long-term creep characteristics of calcareous coral sand under different loading types (single-level and multi-level tests). Based on the experimental results, it is found that calcareous coral sand indeed shows considerable time-dependent creep deformation under a constant stress state. There are two development modes for the volumetric strain versus axial strain curves during creeping under single-level loading; while there is only one development mode under multi-level loading. It is shown that the unfavorable effect of the air entrapped in the micro inner cavities of coral sand particles leads to a spurious volumetric strain measured in the middle and late stages of creep. The determination of the particle size distribution after the tests shows that the relative slippage and rearrangements of sand particles play the leading role in the creep deformation process for calcareous coral sand. The effect of sand particle breakage on creeping is not obvious. Based on these test data, a novel four-parameter mathematical model is proposed to model the creep characteristics of the calcareous coral sand in the South China Sea.

Keywords Calcareous coral sand · Coral reef · Creep characteristics · Creep model · The South China Sea · Triaxial creep test

1 Introduction

Calcareous sand, also known as coral sand, mainly consists of calcium carbonate (the maximum content could exceed 90%) and magnesium carbonate. It is mainly located in the zone from 30° north latitude to 30° south latitude [36, 34], widely distributed in the South China Sea (SCS), the Western Continental Shelf of India, the Northeast, and Northwest Continental Shelf of Australia, and the Caribbean Sea. The calcareous coral sand particles have the characteristics of significant surface roughness, containing inner cavities, irregular shape, easy breakage, etc., which makes the engineering mechanical properties very special compared to the conventional terrestrial quartz sand [51]. In recent years, a series of lands have been built on the top of some natural coral reefs by the means of reclamation in the SCS. The materials used for the reclamation are the calcareous sands extracted from nearby lagoons.

When soil is loaded, it will produce time-independent elastoplastic deformation and time-dependent creep deformation. Understanding the creep deformation characteristics of soil is the precondition for evaluating the post-construction settlement of structures. At present, a lot of work has been carried out on the creep characteristics of

✉ Jianhong Ye
Yejianhongcas@gmail.com; Jhye@whrsm.ac.cn

[1] State Key Laboratory of Geomechanics and Geotechnical Engineering, Institute of Rock and Soil Mechanics, Chinese Academy of Sciences, Wuhan 430071, Hubei, China

[2] School of Safety Science and Emergency Management, Wuhan University of Technology, Wuhan 430070, Hubei, China

[3] Tianjin Research Institute for Water Transport Engineering, M.O.T., Tianjin 300456, China

[4] Xingfa School of Mining Engineering, Wuhan Institute of Technology, Wuhan 430073, Hubei, China

Published online: 16 July 2022

soils. As early as the 1950s, Nishihara [25] proposed a creep model to describe the nonlinear creep deformation of materials, in which a Hooker body, a Kelvin body, and a Bingham body were connected in series. Kondner [11] recognized that the hyperbolic equation could be used to describe the stress–strain relationship of soil. Later, Singh and Mitchell [29] further proposed an empirical stress–strain–time relationship based on some triaxial creep test results. However, this relationship was only applicable in a limited stress range. Additionally, the strain predicted was not zero when the stress was zero. Mesri[22] proposed a creep strain–time relationship adopting a power function based on the assumption that the stress–strain curve was hyperbolic, as proposed by Kondner [11]. Meanwhile, the Burgers creep model was proposed based on the idea that a Maxwell body and a Kelvin body are connected in series [26].

The creep characteristics of soft soils like clay have been widely and comprehensively investigated in the past. Due to the different mechanical properties, the creep characteristics of cohesionless soils under constant stress show significant differences. Many scholars have studied the creep of quartz sands through the one-dimensional consolidation creep test or the triaxial creep test in recent decades. Many mathematical models describing the nonlinear creep characteristics of quartz sands were further proposed, e.g., Murayama [23] and Murayama et al. [24]. Lade et al. [12] conducted a series of drained creep tests to observe the axial creep and volumetric creep of fine quartz sand. It was demonstrated by their results that the creep deformation and plastic deformation were similar in nature. Karimpour and Lade [10] conducted some triaxial creep tests on Virginia quartz sand under different confining pressures, different loading rates to reach the constant stress level, and different deviatoric stress levels to study the relationship between the time effects and particle breakage. It was indicated by their results that under low confining pressure the loading rate basically has no effect on the creep of sand. However, under the condition of high confining pressure, the increase in the loading rate and the stress level will both significantly accelerate the creep deformation of quartz sand. Recently, several experimental works have been conducted on the creep characteristics of terrigenous soil and rock [13–37]. Despite the current development of the research on sand creep, the establishment of creep models and understanding of the creep mechanisms of sandy soil are still the focus of actual research.

It is well known that creep can be related to the particle breakage caused by quasi-static fatigue. After particles breakage, it can further cause the particle's reorganization and slippage. In the recent decade, a series of laboratory tests have been performed to investigate the creep characteristics and the particles breakage of quartz sand (Yang et al. [42], Riaz et al. [28], Wang et al. [33]). Edward et al. [1] conducted one-dimensional consolidation creep tests on non-cemented sand. In their tests, dual resolution high-speed X-ray tomography was adopted to observe the creep process of dry sand. Their study, for the first time, illustrates that the small displacement measured at the boundary is the result of the significant fracturing at the individual grain scale. Liu et al. [17] incorporated the RPT (Rate Process Theory)-based creep model and the probabilistic particle breakage model into a large-scale DEM simulation to study the creep behavior of sand under one-dimensional compression. Their results show that the creep under low deviatoric stress is due to stress redistribution. Meanwhile, the creep under high deviatoric stress is due to the particle reorganization and particle breakage. In addition, a high rolling resistance between particles will lead to a reduction in creep strain.

In the engineering practice in the SCS, many building structures, such as lighthouses, aircraft runways, and revetment breakwater, have been constructed on the reclaimed coral reef lands by taking calcareous coral sand as the foundation material. The creep characteristics of calcareous sand have an important influence on the post-construction behavior of these structures [47]. There have been abundant research works on the mechanical properties of coral sand, such as the cyclic and dynamic strength [27–50], the particles breakage characteristics [30–27], and the static loading properties [48, 39] of calcareous sand. In the recent decade, some attention has been paid to the creep properties [43]. For example, Lade et al. [14] conducted a series of triaxial tests on coral sand. It was found that the inelastic creep deformation behavior of coral sand is different from the traditional plastic deformation characteristics. Lv et al. [19] comparatively conducted some triaxial compression tests on coral sand and silica sand. They found that the volumetric creep, axial creep, and shear creep of coral sand were all significantly greater than that of silica sand. Meanwhile, they adopted a scanning electron microscope to observe the coral sand particles. It was found that the creep of coral sand under general stress condition is mainly caused by the relative movement between sand particles, rather than particles breakage. After that, Wang et al. [35] proposed a rheological model to describe the creep characteristics of calcareous sand based on the test results of Lv et al. [19]. Recently, Sun et al. [30] proposed a fractional creep model for coral sand by incorporating the fractional flow rule and adopting the concept of fractional derivatives. Compared with numerical simulation results, it was found that the model can describe the creep characteristics of coral sand well. Chen et al. [4] conducted one-dimensional compression creep tests under different constant stresses on coral sands with different single-particle

sizes to study the long-term deformation behavior of coral sands sampled from the SCS. It was found that the creep history of coral sand was characterized by three phases, including instantaneous deformation, accelerated deformation, and slow deformation. A two-parameter Weibull distribution function was then found suitable to describe the particle breakage state of coral sand after creep very well.

In summary, there are indeed a number of works that have been previously conducted on the creep of clays, quartz sands, etc. However, with respect to the triaxial creep tests on calcareous coral sand, to the best knowledge of the authors, there are only two valuable pieces of literature available worldwide, i.e., Lade et al. [14] for the calcareous coral sand from the Carib Sea and Lv et al. [19] for the calcareous coral sand from the SCS. Furthermore, there is only a little work on mathematical models describing the creep of calcareous coral sand. To comprehensively understand the creep characteristics of the calcareous coral sand in the SCS, a series of consolidated drained (CD) triaxial creep tests are conducted under different loading ways in this study. Finally, a mathematical model suitable for the creep law of calcareous coral sand in the SCS is proposed based on the experimental data.

2 Test plan

2.1 Basic physical parameters

The calcareous coral sand used in the tests of the present study was sampled from a natural coral reef in the South China Sea. Before testing, all samples were placed in an oven for dehydration at 105 °C for at least 8 h. Each specimen is prepared from a fresh supply of sand. The dry sand is spooned into the cylindrical latex rubber membrane with a thickness of 0.5 mm, which tightly sticks to the inner wall of the specimen mold layer by layer (totally there are 5 layers). The method of knocking the metal specimen mold is adopted to densify the sand, making the surface of each layer reach the preset level in the mold. The diameter of the cylindrical specimens is 61.8 mm and the height is 120 mm. According to the suggestion given by Chinese national regulations, the large particles in the sand need to be removed from these specimens. As a result, there is no particle greater than 5 mm in the sand specimens used in this study. The basic physical parameters of the sand determined from standard tests are listed in Table 1. To ensure the comparability of all test data, a unified particle size gradation is adopted, as shown in Fig. 1. Since $Cu = 6.18$ and $Cc = 1.35$, the calcareous coral sand used is well graded according to the Chinese Code GBJ145-90.

Table 1 Basic physical parameters of the calcareous coral sand (G_s is the specific gravity of sand particles,ρ_{max}, ρ_{min} is the maximum/minimum dry density)

ρ_{max}(g/cm^3)	ρ_{min}(g/cm^3)	G_s	d_{60} (mm)	d_{50} (mm)	d_{30} (mm)	d_{10} (mm)
1.73	1.27	2.83	0.47	0.41	0.22	0.076

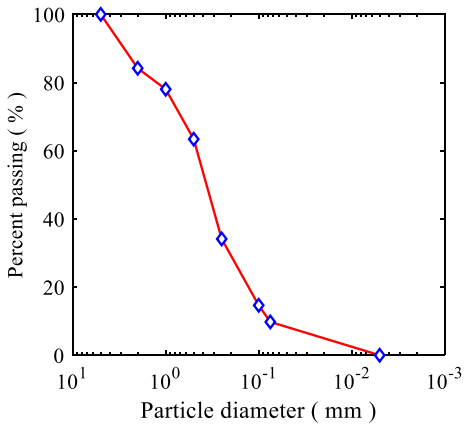

Fig. 1 Particle size gradation curve of the calcareous coral sand sampled from a coral reef in the South China Sea ($Cu = 6.18$, $Cc = 1.35$)

2.2 Test conditions

The tests are conducted on an automatic triaxial apparatus. The loading process of the axial force is divided into two phases. The deviatoric stress is quickly increased to the preset value in the first phase, which is generally within 5 min (Lade et al. [14] concluded that the loading rate effects are not significant for sands). The deviatoric stress is then kept constant in the second phase, controlled by a servo loading system. In this study, there are two ways to apply the axial deviatoric stress: single-level loading and

Table 2 Creep test scheme for calcareous coral sand by the single-level loading way (one specimen, one confining pressure, only one level of deviatoric stress is applied)

Dry density (g/cm^3)	σ_3'(kPa)	q (kPa)					q_f (kPa)
1.45	100	100	200	300	450	600	641
	200	200	400	600	800	1000	1173
	400	400	800	1200	1600	2000	1985
1.65	100	100	200	400	600	800	867
	200	200	400	600	800	1000	1658
	400	500	1000	1500	2000	2500	2502

multi-level loading, respectively. The stress loading schemes are listed in Tables 2 and 3. Single-level loading means that only one level of deviatoric stress is applied to each specimen until its creep deformation reaches a stable state. In this study, the criterion for creep stabilization is that the rate of axial deformation is not greater than 0.005 mm/d. To ensure the comparability of test data between different specimens, it is necessary to use the same equipment to perform the single-level loading tests. Even so, there is no guarantee that the internal structure of each specimen is exactly the same after specimens are prepared. Therefore, it is difficult to satisfy almost identical initial conditions in several creep tests with single-level loading. In the case of multi-level loading, deviatoric stress is step-wise increased on the same specimen. Each level of applied deviatoric stress is kept constant for 3–5 days. Theoretically, the multi-level loading excludes the disadvantage of the single-level tests, because a single sample and thus the same internal structure is tested under different loading conditions. As a result, the test data of the different levels in a multi-level test is more comparable than that obtained from several single-level tests. However, as a possible disadvantage of multi-level loading tests, it should be noted that the loading history in the previous creep phases may have a significant influence on the creeping intensity at the current stress level.

The dry density of the specimens is 1.45 g/cm^3(medium dense sand) and 1.65 g/cm^3(dense sand), which are corresponding to foundation zones treated by the method of vibroflotation on the reclaimed lands in SCS. In this study, 18 standard consolidated drained (CD) triaxial tests (3 parallel tests with 2 dry densities and 3 confining pressures) on saturated calcareous coral sand specimens are firstly conducted, to determine the peak failure strength q_f. The shear rate is set as 0.08 mm/min. The test scheme is listed in Table 4, and the test results are shown in Fig. 2. To improve the saturation of specimens and ensure the reliability of the measured volumetric strain, the combined methods of vacuuming, CO_2 injection, and hydraulic saturation are adopted. The backpressure is set as 200 kPa. The saturation of sand specimens is considered satisfying the requirement when the B value (generally in the range of 0.97–0.997 in this study) is greater than 0.96, like that in Lade et al. [14] and Lv et al. [19]. Otherwise, the specimen will be re-prepared. In the tests, an LVDT displacement sensor (range: 50 mm, resolution: 0.001 mm) is used to record the axial deformation, and a piston-type volumetric controller (range: 250 mL, resolution: 0.001 mL) is used to measure the volume change of specimen by means of the water expelled from or sucked into the saturated specimen.

Table 3 Creep test scheme for calcareous coral sand by the multi-level loading way (one specimen, one confining pressure, and multi-level deviatoric stresses are applied step by step)

Dry density (g/cm^3)	σ_3'(kPa)	q (kPa)				q_f (kPa)
1.45	100	100	200	400	600	641
	200	100	200	400	600	1173
		800				
	400	100	200	400	600	1985
		800	1200	1600		
1.65	100	100	200	400	600	867
	200	100	200	400	600	1658
		800				
	400	100	200	400	600	2502
		800	1200	1600	2000	

3 Test results and analysis

3.1 Axial creep strain–deviatoric stress–time relationship

3.1.1 Single-level loading

The axial creep deformation–time relationships of saturated coral sand measured in the single-level loading tests

Table 4 Standard CD triaxial test program and the measured peak failure strength

Test No	Dry density (g/cm^3)	σ_3'(kPa)	q_f (kPa)	Mean q_f (kPa)
1	1.45	100	616	641
2			638	
3			670	
4		200	1172	1173
5			1143	
6			1204	
7		400	2042	1985
8			1929	
9			1983	
10	1.65	100	861	867
11			889	
12			850	
13		200	1545	1658
14			1701	
15			1727	
16		400	2338	2502
17			2544	
18			2625	

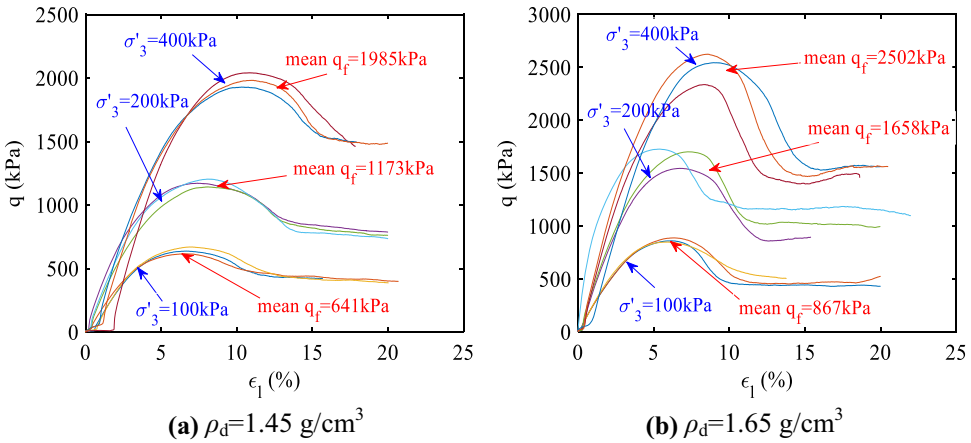

(a) ρ_d=1.45 g/cm^3 **(b)** ρ_d=1.65 g/cm^3

Fig. 2 Stress–strain curves of the calcareous coral sand measured in standard CD triaxial tests (loading rate: 0.08 mm/min)

are shown in Fig. 3. As obvious in Fig. 3, the coral sand indeed undergoes significant creep deformation with time under constant loading of deviatoric stress. The saturated coral sand specimens all undergo attenuated creep under all stress conditions as long as the applied deviatoric stress q is less than the failure strength (creep rate is gradually reduced, rather than increasing with time). There is no steady creep or accelerated creep observed. All the creep curves under different conditions develop similarly with time. The deformations measured in the tests can be divided into two phases: the elastoplastic deformation phase and the creep deformation phase. In the phase of

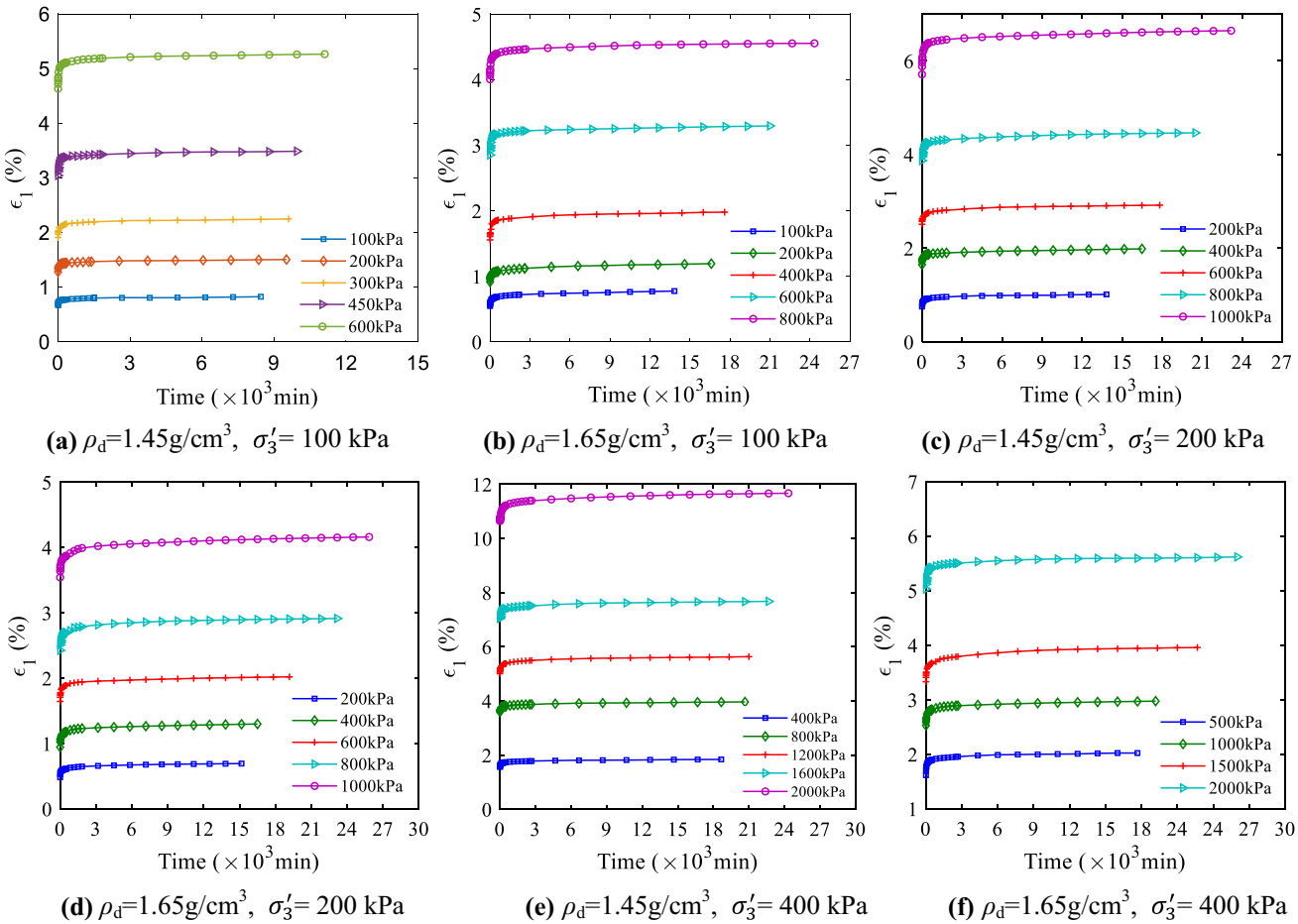

(a) ρ_d=1.45g/cm^3, σ_3'= 100 kPa **(b)** ρ_d=1.65g/cm^3, σ_3'= 100 kPa **(c)** ρ_d=1.45g/cm^3, σ_3'= 200 kPa

(d) ρ_d=1.65g/cm^3, σ_3'= 200 kPa **(e)** ρ_d=1.45g/cm^3, σ_3'= 400 kPa **(f)** ρ_d=1.65g/cm^3, σ_3'= 400 kPa

Fig. 3 Creep curves of saturated calcareous coral sand (single-level loading)

elastoplastic deformation, the particles of the sand specimens are continuously adjusted and rearranged during the application of the target deviatoric stress. Sand specimens are rapidly compressed and the strain rate is relatively high in the phase of elastoplastic deformation, resulting in the initial strain ε_0. In the creep deformation phase, the relative position of particles inside sand specimens continues to be adjusted and rearranged under the constant deviatoric stress. The deformation rate of sand specimens keeps decreasing and finally approaches 0 over time. During this process, the axial strain of the sand specimens only increases slowly, producing the creep strain ε_c. Creep deformation generally accounts for 8%–30% of the total deformation (see Appendix 1). It is indicated that the creep deformation of coral sand is considerable. However, there is no significant mathematical correlation between the percentage of creep deformation and the dry density, confining pressure $\sigma_3^{'}$, and deviatoric stress q. However, there are qualitative relationships between them. Under the same confining pressure, the axial creep deformation of medium dense sand is greater than that of dense sand. It is due to the fact that the looser the sand is, the more pore space exists, and the easier it is to be compressed, and vice versa. For the sand specimens with the same confining pressure and dry density, the greater the deviatoric stress, the greater the creep deformation. The time for the creep deformation to become stable (creep strain < 0.005 mm/d) is generally more than 10 days. When the sand is denser and the confining pressure is greater, or the applied deviatoric stress is greater, the creep deformation needs more time to become stable (creep strain < 0.005 mm/d). For example, the creeping time of the coral sand with a dry density of 1.45 g/cm^3 is about 10 days when q = 100 kPa is applied under σ_3'= 100 kPa, while for the coral sand with a dry density of 1.65 g/cm^3, it is about 19 days when q = 2000 kPa is applied under $\sigma_3^{'}$ = 400 kPa. The reason is that the denser the sand is or the greater the applied stress is, the less space is left for the particles to adjust their relative positions in the creep deformation stage. Meanwhile, the denser the sand is or the greater the applied stress is, the greater the shear-bearing capacity of the sand, resulting in a smaller slipping rate between particles. Therefore, it must take a longer time to reach a new equilibrium state.

3.1.2 Multi-level loading

The stress–axial creep strain–time relationship of saturated calcareous coral sand measured in the multi-level loading tests is shown in Fig. 4. As illustrated in Fig. 4, it is

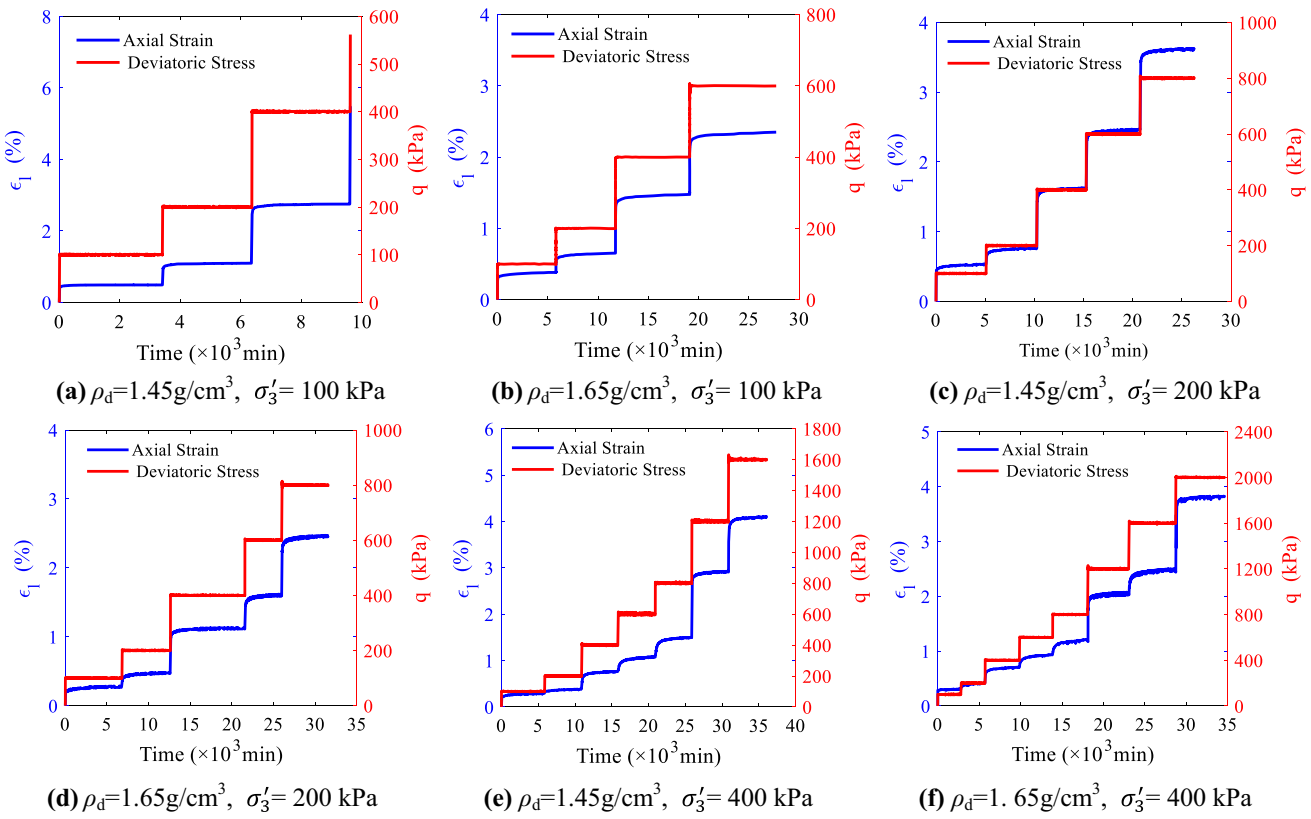

Fig. 4 Creep curves of saturated calcareous coral sand (multi-level loading)

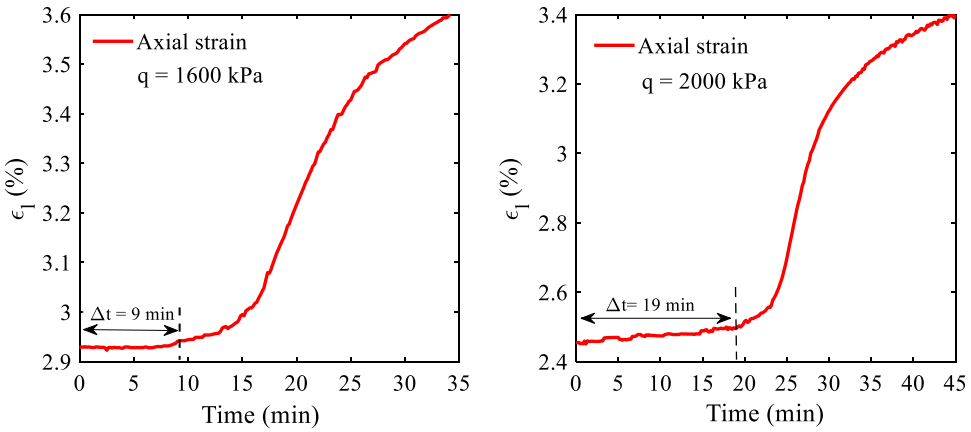

(a) ρ_d=1.45g/cm^3, σ_3'= 400 kPa **(b)** ρ_d=1.65g/cm^3, σ_3'= 400 kPa

Fig. 5 Time lag effect of creep deformation of calcareous coral sand (multi-level test)

observed that the creep deformation of coral sand develops with time under each level of constant deviatoric stress. Under the same confining pressure, the axial creep deformation of the specimens with a greater dry density is less. Under the condition of the same dry density, the greater the confining pressure, the less axial deformation develops. The time-independent elastoplastic deformation of coral sand specimens occurs as each level of deviatoric stress is quickly applied. The creep deformation appears to occur when the deviatoric stress reaches its preset value. After this moment, the creep continuously becomes slower over time. Creep deformation generally accounts for 7%–90% of the total deformation (see Appendix 2). Different from the single-level loading tests, only when the deviatoric stress is close to the failure strength, the coral sand specimens, regardless of density state, hardly deform after they are rapidly loaded to the preset deviatoric stress when σ_3'= 400 kPa. After some time (about 9 min for medium dense sand and 19 min for dense sand), the creep rate suddenly increases, showing a "time-lag effect of creep deformation," as shown in Fig. 5. The reason is that the sand specimens are continuously compacted in the process of applying the deviatoric stress level by level under a high confining pressure (Noted: this phenomenon is only observed when σ_3'= 400 kPa). As a result, the ability of the coral sand to resist deformation is becoming stronger and stronger. Namely, strong structuration is gradually formed in the inner structure of the specimen. When the deviatoric stress is close to the failure strength, the coral sand specimens can bear great stress without deformation in a short time. The denser the sand specimen is, the longer the deformation lagging time is. Due to the application of a greater deviatoric stress, the stable state formed in the sand specimens during the creep phase under the last level of stress tends to become unstable again. The sand particles move and slip on each other again, and their relative positions are rearranged again. As a result, a rapid deformation will occur. After some time, the deformation rate gradually slows down, presenting an attenuation characteristic. Another interesting phenomenon observed during the loading phases is shown in Fig. 6 for a sample with a dry density of 1.45 g/cm^3 and σ_3'= 100 kPa. The specimen does not deform at the beginning, and maintains this state for about 130 s, in the process that the deviatoric stress q is linearly loaded from q = 400 kPa to q = 600 kPa. However, the deformation starts to develop at q = 543 kPa. Then, the shear failure of the specimen occurs at the deviatoric stress of q = 593 kPa. At this moment, the specimen is not destroyed instantaneously. Instead, it bears the peak deviatoric stress for about 20 s before the specimen fails, presenting the "time-lag effect of failure," as shown in Fig. 6. The above-mentioned two time-lag effects have not been reported in previous literature, because the CD triaxial creep tests under multi-level loading have not been previously conducted on calcareous coral sand, so far to the best knowledge of the authors.

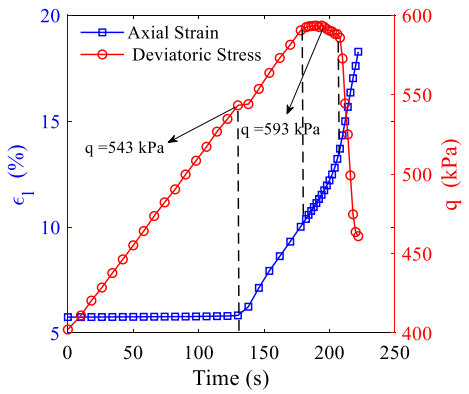

Fig. 6 Time lag effect of failure when ρ_d = 1.45 g/cm^3, σ_3'= 100 kPa (multi-level test)

The relationships of creep deformation versus time are shown in diagrams with a double logarithmic scale in Fig. 7. The same data as in Figs. 3 and 4 is shown. According to "Boltzmann linear superposition principle" [21] (It proposed that each level of stress loading will independently contribute to the deformation of materials in the creep process, and the total creep is the linear sum of the creep deformation caused by each level of loading), to ease the comparison with the results under single-level loading, the creep curves from the multi-level loading tests, shown in Fig. 7c and d, have been divided into the same form as the curves under single-level loading, as shown in Fig. 7a and b. It is observed that the initial elastoplastic strains of calcareous coral sand with the same dry density and confining pressure under single-level loading are generally greater than those under multi-level loading at each level of deviatoric stress. This is because the specimens are seriously affected by the previously applied stresses in multi-level tests. It is further observed that, under the conditions of the same dry density and confining pressure, all the curves in the double logarithmic coordinates system are approximately linear and parallel to each other. It means that the creep strain–time curves will be approximately overlapped if the initial elastoplastic strains are excluded under the conditions of the same dry density and confining pressure. It is indicated that the magnitude of the applied deviatoric stress during creeping has no significant effect on the slope of the creep strain–time curves. We must emphasize the "approximation" here, because they are actually not strictly straight lines, and they are also not strictly parallel to each other.

3.2 Volumetric strain–axial strain during creeping

3.2.1 Single-level loading

The relationships between the volumetric strain ε_v and axial strain ε_1 of the coral sand specimens recorded in the single-level tests are illustrated in Fig. 8. Each curve has been divided into two sections by a small vertical dashed line in Fig. 8, corresponding to the elastoplastic

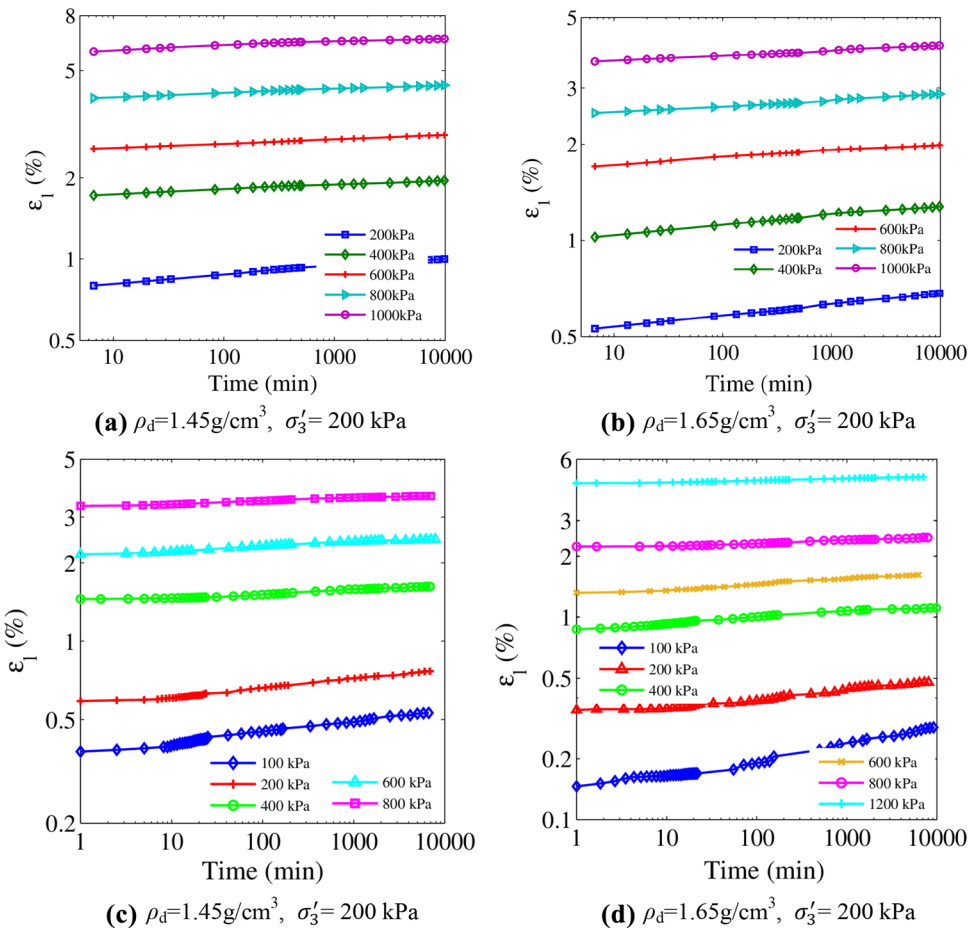

Fig. 7 Creep strain–time curves of calcareous coral sand in diagrams with double logarithmic scale (**a** and **b**: single-level loading, **c** and **d**: multi-level loading. The values in the legend specify the applied deviatoric stress during creep)

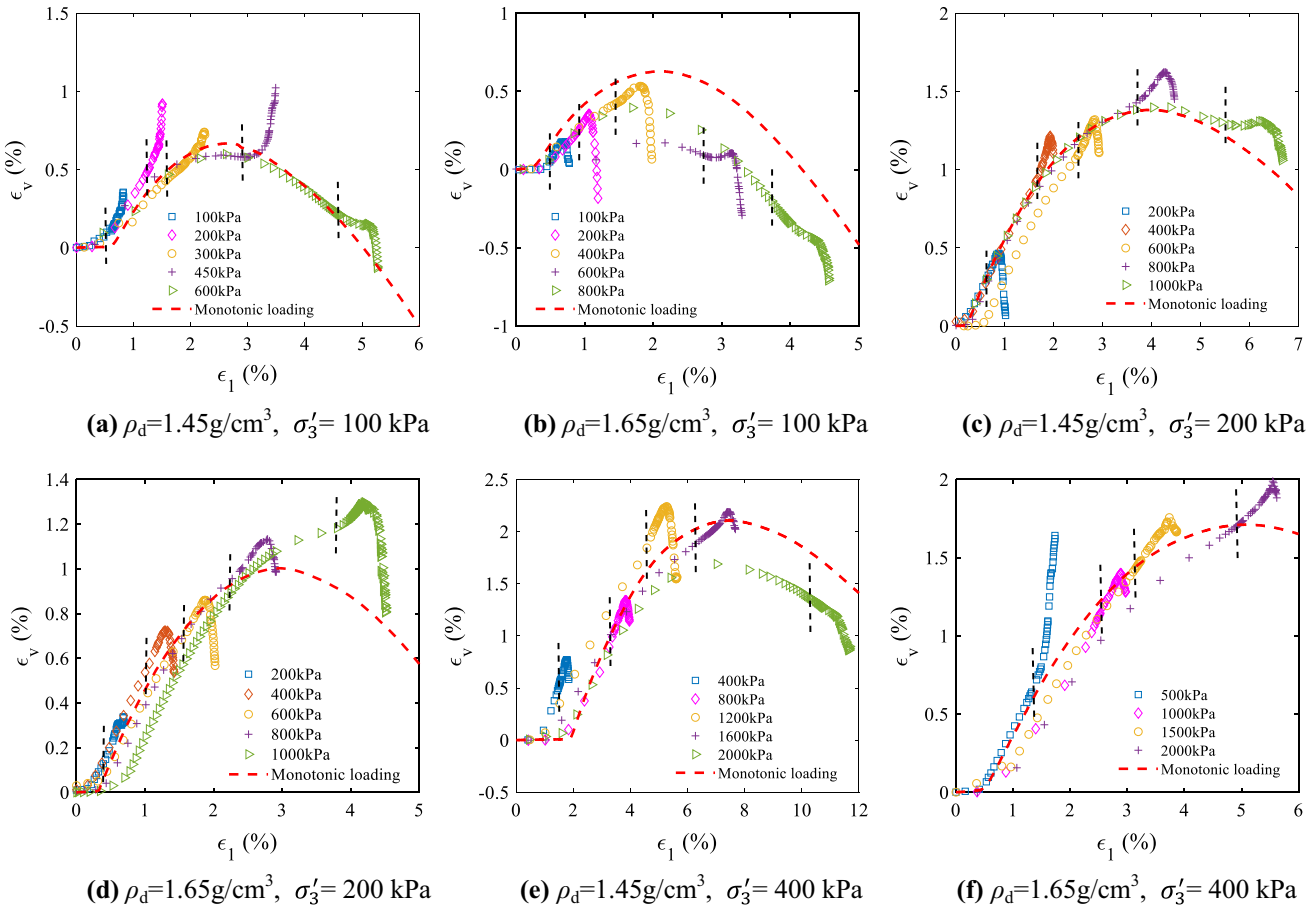

(a) ρ_d=1.45g/cm^3, σ_3'= 100 kPa **(b)** ρ_d=1.65g/cm^3, σ_3'= 100 kPa **(c)** ρ_d=1.45g/cm^3, σ_3'= 200 kPa

(d) ρ_d=1.65g/cm^3, σ_3'= 200 kPa **(e)** ρ_d=1.45g/cm^3, σ_3'= 400 kPa **(f)** ρ_d=1.65g/cm^3, σ_3'= 400 kPa

Fig. 8 Volumetric strain versus axial strain of calcareous coral sand (single-level loading) (Noted: the vertical dotted lines separate the initial elastoplastic loading and the following creep stage)

deformation in the initial loading phase and the subsequent creeping phase, respectively. Furthermore, the $\varepsilon_v - \varepsilon_1$ curves recorded in the monotonic standard triaxial CD tests corresponding to Fig. 2 are also presented in Fig. 8, for the convenience of the discussion on the development of the volumetric strain during creeping. It should be noted that these $\varepsilon_v - \varepsilon_1$ curves recorded in the monotonic CD tests show some deviation from those measured in the loading phase of the single-level tests performed with the same dry density and confining pressure, due to the natural scatter of experimental data and a slightly different structure of each specimen used resulting from the preparation process. The monotonic test data can thus just serve as an approximate reference in the following analysis.

In Fig. 8, it is observed that the $\varepsilon_v - \varepsilon_1$ curves in the initial loading phase before creeping basically follow the counterparts recorded in the monotonic CD tests. However, there are three types of development modes for the $\varepsilon_v - \varepsilon_1$ curves during creeping: (1) The first mode is only contractive, see, e.g., the $\varepsilon_v - \varepsilon_1$ curves when q = 100, 200, 300, and 450 kPa in Fig. 8a, as well as that when q = 500 kPa in Fig. 8f. (2) The second mode is contractive firstly and then dilative. Most of the $\varepsilon_v - \varepsilon_1$ curves during creeping illustrated in Fig. 8 belong to this type of mode. (3) The third mode is only dilative from the beginning, see, e.g., the $\varepsilon_v - \varepsilon_1$ curves when q = 600 kPa in Fig. 8a, when q = 600, 800 kPa in Fig. 8b, and when q = 2000 kPa in Fig. 8e. However, it is found that the $\varepsilon_v - \varepsilon_1$ curves during creeping for the third mode can generally be divided into two parts, with a significantly larger slope of the $\varepsilon_v - \varepsilon_1$ curves in the second creep stage.

Based on the experimental data, the conditions for the occurrence of the three types of development modes of $\varepsilon_v - \varepsilon_1$ curves during creeping can be identified. If the axial strain ε_1 at the end of the initial loading phase (corresponding to the vertical dotted line in Fig. 8) is not significantly larger than the ε_1 at the phase transformation point (corresponding to the change from contractive to dilative response in the monotonic CD tests), the first or second development mode for the $\varepsilon_v - \varepsilon_1$ curves during creeping will generally occur. Otherwise, that means if the specimen already shows a dilative response during the loading to the target deviatoric stress, the third development mode will occur.

It can be seen that the second development mode of the $\varepsilon_v - \varepsilon_1$ curves during creeping is very common in the single-level loading tests. Its significant difference from the first development mode is that the development of volumetric strain will change from contractive to dilative at the middle and later creep stage, and the axial creep strain is significantly smaller than the volumetric creep strain developing in this dilative stage. It results in relatively large slopes of the $\varepsilon_v - \varepsilon_1$ curves. This phenomenon was not observed by Lade et al. [14] and Lv et al. [19] but has been clearly displayed by the test data of Liu et al. [18]. However, the latter authors did not pay attention to this fact, and did not explain the occurrence mechanism for this phenomenon. In the following, a possible explanation of this phenomenon is given from the perspectives of specimen saturation, and the micro-structures of coral sand particles.

To identify a possible effect of the degree of saturation of the specimen, corresponding to the B value, on this observed phenomenon, another CD triaxial creep test was conducted on a calcareous coral sand specimen (ρ_d = 1.65 g/cm^3) with a much higher back pressure of 1000 kPa to further improve the saturation of the specimen (test condition: q = 600 kPa and σ_3'= 200 kPa). The time history of the axial strain, and the $\varepsilon_v - \varepsilon_1$ curves recorded in this test are compared to those from a similar test with a lower back pressure of 200 kPa in Fig. 9. It should be noted that the B value of the specimens corresponding to Fig. 9a and b is 0.990 and 0.997, respectively, which is very close to 1.0. It is indicated that the test operation for specimen saturation in this study is in the line with the test requirements, and that a greater B value is more likely to be obtained under higher back pressure. In Fig. 9, it is observed that the development processes of ε_1-t and $\varepsilon_v - \varepsilon_1$ under different back pressures are similar. The volumetric responses are both contractive at first (corresponding to the quick creep phase), and then dilative in the middle and late creep stage (corresponding to the slow creep phase). The observed significant difference is that the maximum dilative $\Delta\varepsilon_v$ is 0.39% when B = 0.990, while it is only 0.12% when B = 0.997. It seems that the dilative trends indeed are negatively related to the saturation degree of specimen. However, the physical reason for the transformation from contractive to dilative response during creeping remains unclear, because it happens in Fig. 9a and b under different B values, even though they are both close to 1.0. Based on this recognition, it may be concluded that the second development mode of $\varepsilon_v - \varepsilon_1$ curves during creeping may occur even if the B value suggests a very high degree of saturation of the specimens. Therefore, knowing the B value alone seems not to be sufficient to predict the kind of volumetric response during the creep phase.

To explore the effect of the micro-structure of calcareous coral sand on the occurrence of the second development mode of $\varepsilon_v - \varepsilon_1$ curves during creeping, another CD

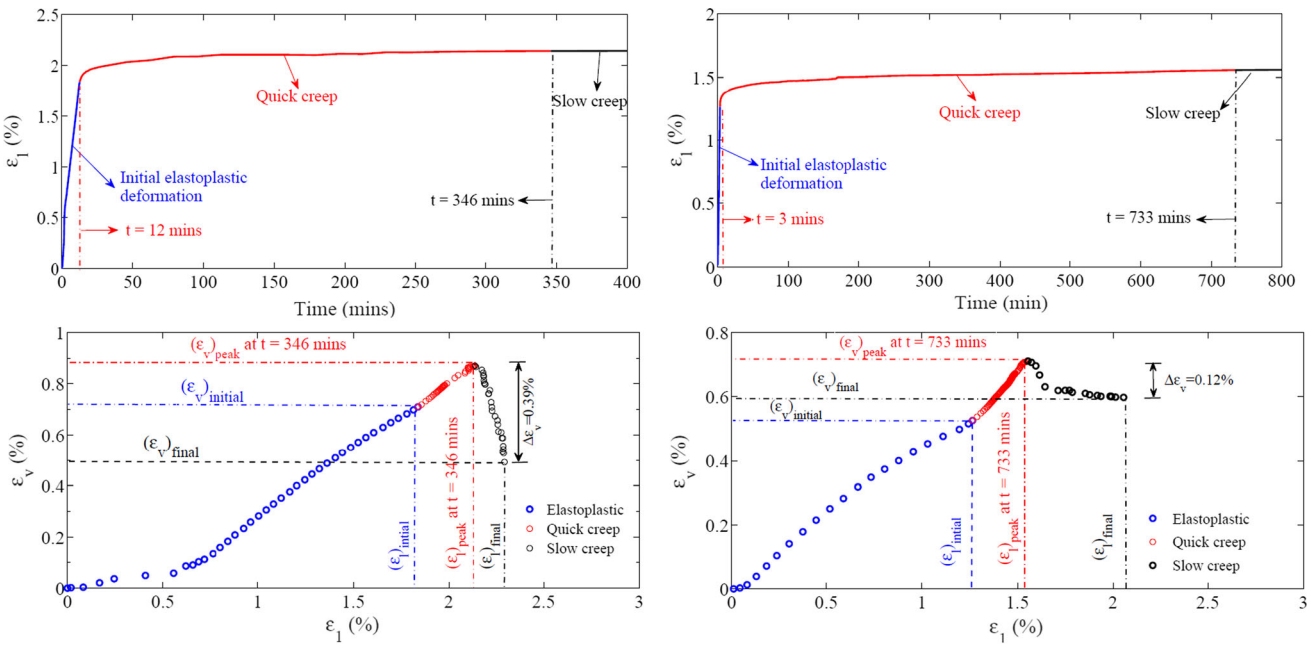

(a) Back pressure=200 kPa (B=0.990) **(b)** Back pressure=1000 kPa (B=0.997)

Fig. 9 Experimental relationships of ε_1-t and $\varepsilon_v - \varepsilon_1$ for calcareous coral sand under different back pressures when q = 600 kPa, σ_3'= 200 kPa, and ρ_d = 1.65 g/cm^3 (It is noted that the definitions for the quick creep phase and slow creep phase are only relative or qualitative. In this figure, they are differentiated by the transition from contractive to dilative volumetric response during creep)

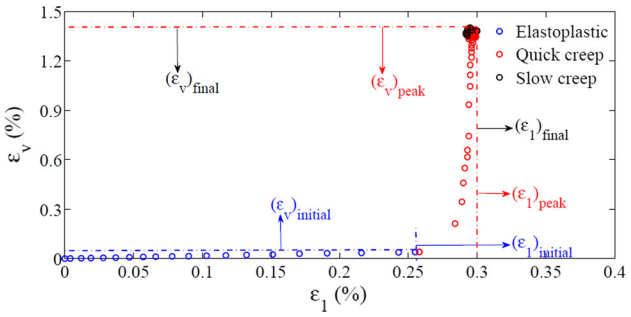

Fig. 10 Experimental relationships of $\varepsilon_v - \varepsilon_1$ for Fujian standard quartz sand with the single particle diameter of 0.5–1 mm under back pressures = 1000 kPa when q = 600 kPa, σ_3'= 200 kPa, and ρ_d = 1.0 g/cm^3 (B = 0.996)

triaxial creep test was conducted on Fujian standard quartz sand (a type of standard sand produced in China) in this study. The experimental $\varepsilon_v - \varepsilon_1$ curve for the Fujian standard quartz sand is shown in Fig. 10. It is clearly observed that there is basically no dilative response in the slow creep phase for quartz sand, which is completely different from that for calcareous coral sand. It is indicated that the observed phenomenon of the transformation from contractive to dilative behavior in the second development mode of $\varepsilon_v - \varepsilon_1$ curves during creeping are closely related to the type of sand. Further analysis indicates that the occurrence of the transformation from contractive to dilative response for calcareous coral sand may be caused by the fact that there are a great number of micro inner cavities in the sand particles, as illustrated in Fig. 11a. Just because there are basically no micro inner cavities in quartz sand particles, like that in Fig. 11b, there is no transformation from contractive to dilative response in the slow creep phase for the Fujian standard quartz sand, as demonstrated in Fig. 10.

The influencing mechanism of these micro inner cavities in the sand particles of coral sand is illustrated in Fig. 12. It has been well known that there are a great number of micro inner cavities in coral sand particles. The diameters of these inner cavities generally are in the range from a few microns to a dozen microns, as shown in Fig. 11a. Because of the surface tension of pore water, it is basically impossible for pore water to fully fill these inner cavities during specimen saturation, resulting in that there is more or less air that is trapped in the inner cavities, as illustrated in Fig. 12 (a). Under the condition of higher back pressure, the compressibility of this trapped air will be less than that under low back pressure. Under the continuous action by the back pressure, a time-dependent volumetric contraction of the trapped air in these inner cavities occurs (also can be referred to as volumetric creep). As a result, more pore water gradually gets into these inner cavities, as illustrated in Fig. 12b. To remain the back pressure which has been set as a constant throughout the whole testing, the piston-type volumetric controller has to gradually inject more water into the specimen. According to the conventional analysis of the data recorded by a piston-type volumetric controller, this volume change would wrongly be attributed to a dilation of the specimen in the middle and late stages of creep. However, the particles' skeleton of the coral sand specimen does not dilate in the two creep stages. Therefore, the dilatancy measured by the piston-type volumetric controller in the middle and late creep stages for calcareous coral sand is actually some kind of fake data. Because inner cavities are naturally existing in the sand particles of coral sand, the problem pointed out above is theoretically difficult to be avoided. Finally, our recognition is that the dilative ε_v chronically measured by a piston-type volumetric controller in the middle and late stage of creep is invalid. However, the measured data in the early stage of creep is still reliable because the time-dependent volumetric contraction of the trapped air seems to be rather insignificant in this creep stage. Overall, it is suggested to adopt other methods, such as the cricoid LVDT sensor strapping the specimen or the non-contact optical DIC measurement, to measure the ε_v of calcareous coral sand with inner cavities occurring in the middle and late creep

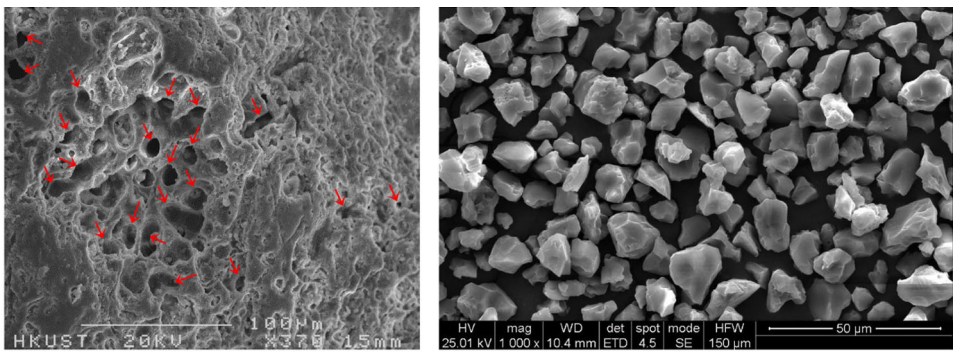

(a) Calcareous coral sand with inner cavities **(b)** Typical quartz sand without inner cavity

Fig. 11 SEM photographs of the calcareous coral sand used in this study, as well as typical quartz sand (Zuo et al. [52])

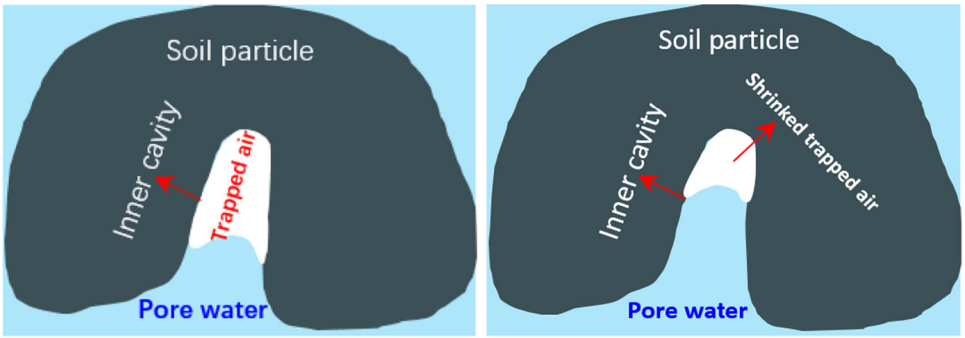

(a) In the early stage of creep **(b)** In the middle and late stage of creep

Fig. 12 Mechanism illustration of the volumetric dilation process in the later stage of creep for calcareous coral sand

stage. For quartz sand without inner cavity, the conventional method involving a piston-type volumetric controller can still be used.

Based on the above analysis, it is found that the second development mode of the $\varepsilon_v - \varepsilon_1$ curves during creeping is actually the same as the first development mode, if the spurious data of the dilative ε_v in the middle and late creep stage caused by the inner cavities in coral sand particles is excluded. Finally, it may be concluded that there are only two types of development modes for the $\varepsilon_v - \varepsilon_1$ curves during creeping for the calcareous coral sand in the South China Sea. The first mode is that there is only contraction during creeping if the axial strain ε_1 at the end of the initial loading stage (corresponding to the vertical dotted line in Fig. 8) is not significantly larger than the ε_1 at the phase transformation point. Otherwise, there is only continuous dilation during creeping. It should be noted that it is yet difficult to give a quantitative description for the above statement "not significantly more than" so far, based on the test data in this study. More experimental works are needed in the future.

After the spurious data of the dilative ε_v in the middle and late creep stage being excluded, it is found in Fig. 8 that the $\varepsilon_v - \varepsilon_1$ curves during creeping are generally not consistent with those recorded in monotonic tests. It is indicated that the potential surface in the p'-q coordinate system for creep strain is different from that for elasto-plastic strain for calcareous coral sand. Therefore, the potential surface for elastoplastic strain cannot be copied when developing visco-elastoplastic constitutive models for calcareous coral sand. This recognition is completely different from that made by Lade and Liu [13] for quartz sand, who claimed that the potential surface could be shared for the creep strain and elastoplastic strain.

Since the calcareous coral sand used in this study generally has inner cavities in the particles, there should be a spurious transformation from contractive to dilative ε_v response in the middle and late creep stage for all specimens, according to the above-explained mechanism. However, there are also tests where this effect has not been observed, e.g., the specimen under q = 500 kPa in Fig. 8f. Currently, the reason is hard to be given and needs more research work in the future.

3.2.2 Multi-level loading

The volumetric strain–axial strain relationship under each level of deviatoric stress measured in the multi-level loading tests is shown in Fig. 13. Similarly, each curve has been divided into two sections by a small vertical dashed line in Fig. 13, corresponding to the initial elastoplastic strain and the creep strain, respectively.

In Fig. 13, it is observed that similar to the findings of the single-level tests, there are also two types of development modes for the $\varepsilon_v - \varepsilon_1$ curves during creeping. The first type is that there is only volumetric contraction during creeping under each level of q, such as that illustrated in Figs. 13a, e and f. The second type is that the ε_v is first contractive, and then becomes dilative in the middle and late stage of creep under each level of q, such as that illustrated in Fig. 13b, c and d. The mechanism for this spurious transformation from contractive to dilative must be the same as that occurring in the above single-level tests. Furthermore, the dilative increment of ε_v is generally most significant under the first level of q. It will produce a profound effect on the development of the $\varepsilon_v - \varepsilon_1$ curves during creeping under the subsequent levels of q. If the spurious data of the dilative ε_v in the middle and late creep stage is excluded, it is found that there is only volumetric contraction during creeping under all levels of q for each specimen used in multi-level loading tests, even though several levels of q are close to the corresponding peak strength q_f, which have been listed in Table 2.

Similar to the single-stage tests, it is unclear so far why the transformation from contractive to dilative behavior does not occur for three of the tests shown in Fig. 13a, e

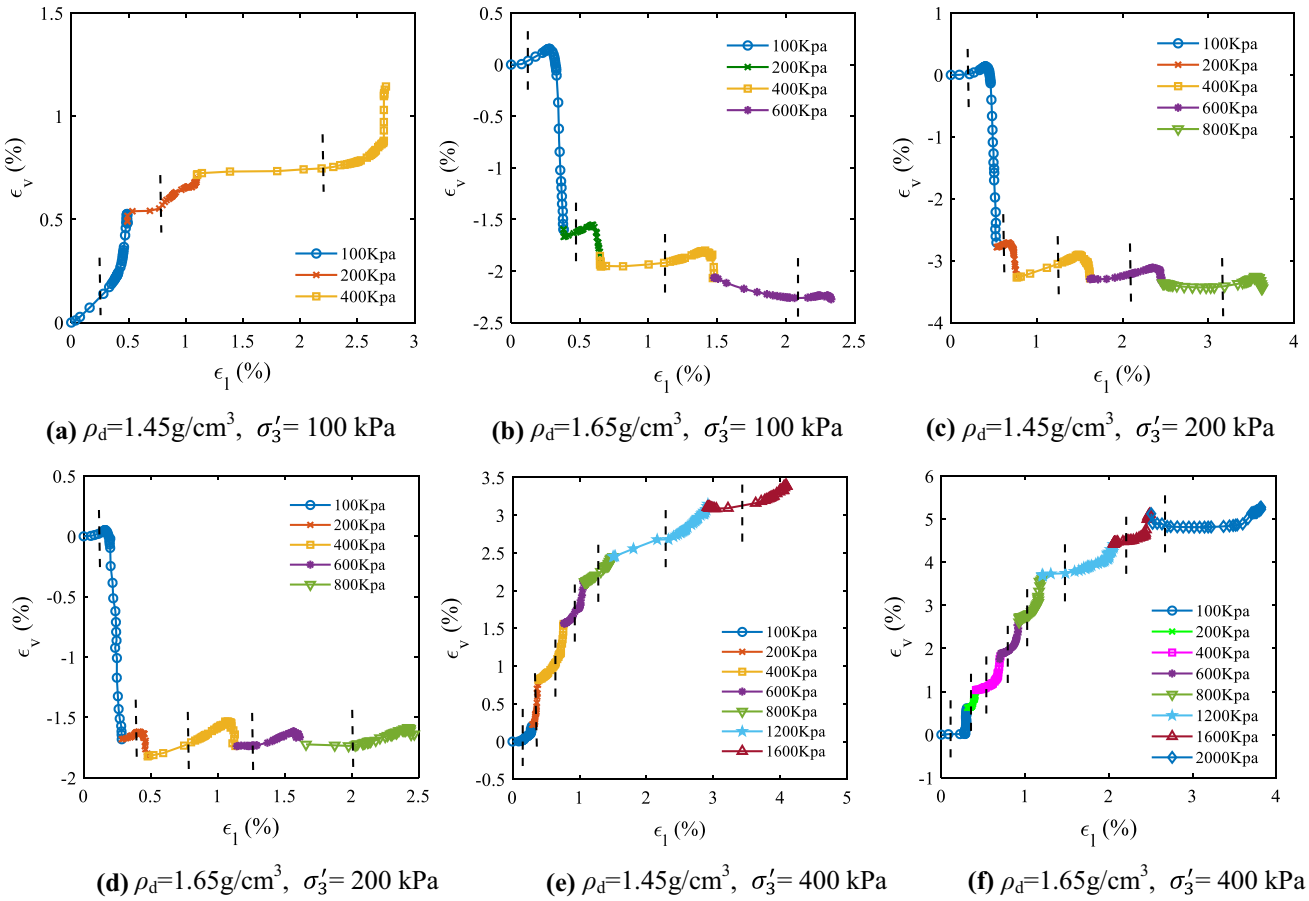

(a) ρ_d=1.45g/cm^3, σ_3'= 100 kPa **(b)** ρ_d=1.65g/cm^3, σ_3'= 100 kPa **(c)** ρ_d=1.45g/cm^3, σ_3'= 200 kPa

(d) ρ_d=1.65g/cm^3, σ_3'= 200 kPa **(e)** ρ_d=1.45g/cm^3, σ_3'= 400 kPa **(f)** ρ_d=1.65g/cm^3, σ_3'= 400 kPa

Fig. 13 Volumetric strain versus axial strain of calcareous coral sand (multi-level loading) (Noted: the vertical dotted lines separate the initial elastoplastic and creep stage; the values in the legend are the deviatoric stresses of the current level)

and f, although all sand particles of the calcareous coral sand used in this study contain inner cavities. This question still needs more comprehensive research works in the future.

3.3 Creep mechanism

There are generally two types of mechanisms for the creep of sandy soil. They are relative position adjustment between particles and particle breakage, respectively. To explore the creep mechanism of the calcareous coral sand used in this study, a series of particle size gradation tests have been performed before and after the creep tests for each specimen to quantitatively study the particle breakage characteristics, and to judge its contribution to the creep deformation. The particle size gradation curves of calcareous sand before and after creep tests all are illustrated in Fig. 14.

The creep phenomenon of sandy soil has been previously demonstrated as the development of time-dependent deformation at the macro level, induced by the sliding and rolling of particles on their contact surfaces, as well as by the crushing of particles at the micro-level. Particle breakage is usually considered to be closely related to the creep of granular materials. For example, Karimpour and Lade [10] found that particle breakage played an important role in the creep deformation of quartz sand; while the particle rearrangement and frictional sliding between particles have little effect on the creep under high-stress condition. The work conducted by Brzesowsky et al. [2] indicated that there was subcritical transgranular fragmentation occurring in the creep process of quartz sand, and accompanied by the sliding and the rearrangement between particles. Lv et al. [19] found that the creep of coral sand was mainly caused by the sliding and rearrangement of particles under low-stress condition (< 800 kPa), while the particle breakage was significant under the condition of high stress (≥ 800 kPa). Wang et al. [35] found that there were a large number of internal pores in coral sand particles, and there was significant stress concentration occurring near these pores during creeping, which would lead to the occurrence of particles breakage.

As illustrated in Fig. 14a–f for the single-level tests, the amount of particle breakage is actually not large. Only the

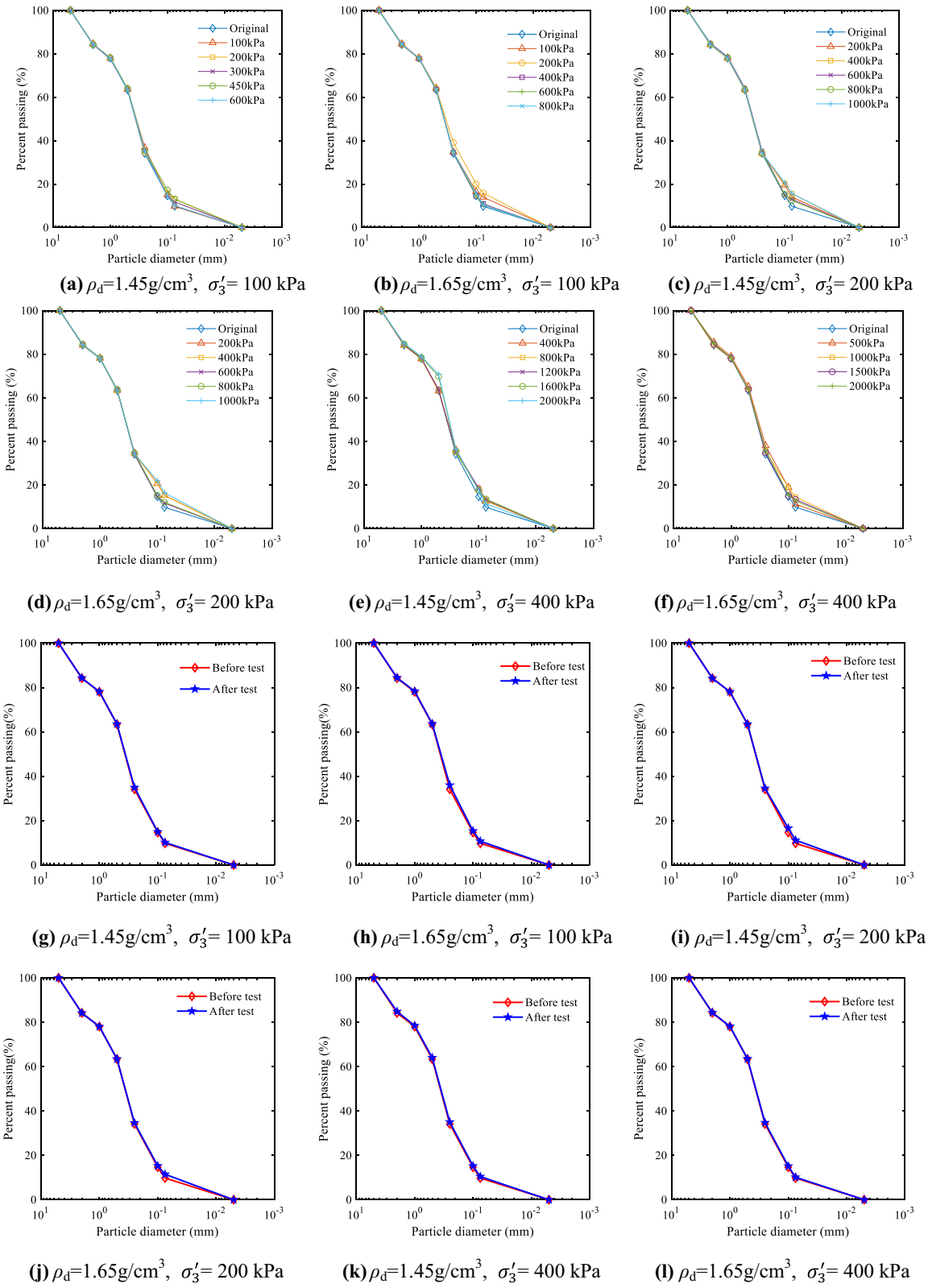

(a) ρ_d=1.45g/cm^3, σ_3'= 100 kPa **(b)** ρ_d=1.65g/cm^3, σ_3'= 100 kPa **(c)** ρ_d=1.45g/cm^3, σ_3'= 200 kPa

(d) ρ_d=1.65g/cm^3, σ_3'= 200 kPa **(e)** ρ_d=1.45g/cm^3, σ_3'= 400 kPa **(f)** ρ_d=1.65g/cm^3, σ_3'= 400 kPa

(g) ρ_d=1.45g/cm^3, σ_3'= 100 kPa **(h)** ρ_d=1.65g/cm^3, σ_3'= 100 kPa **(i)** ρ_d=1.45g/cm^3, σ_3'= 200 kPa

(j) ρ_d=1.65g/cm^3, σ_3'= 200 kPa **(k)** ρ_d=1.45g/cm^3, σ_3'= 400 kPa **(l)** ρ_d=1.65g/cm^3, σ_3'= 400 kPa

Fig. 14 Particle size gradation curves of calcareous coral sand before and after creep tests (**a**–**f**): single-level loading, (**g**–**l**): multi-level loading)

particles with an equivalent diameter of less than 0.1 mm present a small amount of crushing when σ_3'= 100 kPa. Therefore, it is concluded that the creep of coral sand under low confining pressure is mainly caused by the sliding and the rearrangement of particles. When σ_3'= 400 kPa, a certain degree of particle breakage is observed for the particles with a size of less than 1 mm. It is indicated that the creep of calcareous coral sand under high stress is not only due to the sliding and rearrangement between particles but also due to the breakage of a small number of sand particles. Overall, there is no obvious regularity for the particle size gradation curves determined after the creep test with the increasing of the applied deviatoric stress under the condition of the same dry density and the same confining pressure. It is indicated that the breakage of calcareous coral sand particles is of minor importance when $\sigma_3' \leq$ 400 kPa. Compared to the experimental results under the condition of single-level loading (Fig. 14a–f), the particle breakage is even less pronounced under the condition of multi-level loading (Fig. 14g–l). Finally, it can be concluded that the creep of calcareous coral sand with a natural particle size gradation from the SCS is mainly caused by the sliding and the rearrangement of sand particles under low-stress conditions. This recognition is nearly the same as that observed by Lv et al. [19], in which also specimens with a natural particle size gradation were used. Creep triaxial tests under very high confining pressure which is greater than 2 MPa could be further conducted to investigate the contribution of particle breakage to the creep of calcareous coral sand at those high-stress levels in the future. It is necessary to notice that the particle breakage of coral sand is claimed relatively significant in monotonic triaxial tests in some recent literature [38, 32]. The main reason could be that the specimens with single particle size greater than 0.5 mm, rather than a natural particle size gradation were used in these tests. As is well known, the specimens with single particle size greater than 0.5 mm are much more prone to generate particle crushing than those with a natural particle size gradation.

4 Creep mathematical model

To predict the long-term settlements of structures built on calcareous coral sand, a creep constitutive model is necessary which describes the stress–strain–time relationship of soil. Currently, the Mesri model (Mesri [22]) and the Burgers model [26] are widely used to describe the creep deformation behavior of soil. As addressed above, the Mesri model assumes a hyperbolic stress–strain curve for the loading phase, as proposed by Konder [11], and the relationship between creep strain and time is described by a power function. Actually, the precondition assumption of the Mesri model is not consistent with reality. Therefore, the reliability of the Mesri model should be less than that of element-based models consisting of Maxwell body and/or Kelvin body, such as the Burgers-types models. This study will further modify a Burgers creep model for calcareous coral sand based on our experimental results.

Original Burgers creep model was obtained by connecting a Maxwell body (a purely viscous damper and a spring in parallel) and a Kelvin body in series. To describe the nonlinear creep deformation of materials, Yin et al. [44] proposed a new creep element, called as "soft-matter element." This type of element could be adopted to describe the deformation characteristics of the material between an ideal solid and an ideal fluid, see Fig. 15. Under the action of constant stress, the deformation described by this type of element will neither increase linearly as the ideal fluid nor be kept as constant as the ideal solid. If the viscous damper in Maxwell's body is replaced by the soft-matter element, the original Burgers model is modified into a new form, referred to as the Burgers soft-matter model.

Based on the theory of fractional derivative, He et al. [9] described the viscous damper in the Burgers soft-matter model, and proposed the following stress–strain–time equation:

$$\varepsilon_1 = \frac{q}{E_0} + \frac{q}{E_1}\left(1 - e^{-\frac{E_1}{\eta_1}t}\right) + \frac{q}{\xi}\frac{t^{\beta}}{\Gamma(1+\beta)} \tag{1}$$

where E_0 and E_1 are the deformation modulus of the springs in the Hook body and the Kelvin body, respectively, η_1 is the viscosity coefficient, ξ and β are the parameters of the soft-matter element. When $\beta = 0$, the soft element degenerates into a spring, which represents an ideal solid. When $\beta = 1$, the soft element becomes a damper, which represents an ideal fluid. The form of Eq. (1) can be rewritten as:

$$\varepsilon_1 = \frac{q}{E_0} + \frac{q}{E_1}\left(1 - e^{-Rt}\right) + \frac{q}{C}t^{\beta} \tag{2}$$

where $R = E_1/\eta_1$, $C = \xi \times \Gamma(1+\beta)$. q/E_0 represents the time-independent initial elastoplastic deformation. The latter two items in Eq. (2) are the creep deformation. It is noted that the original Burgers model is just a special case

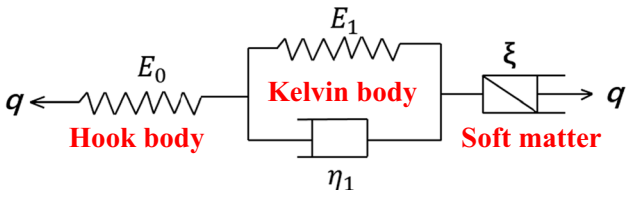

Fig. 15 Elements composition of Burgers soft-matter model

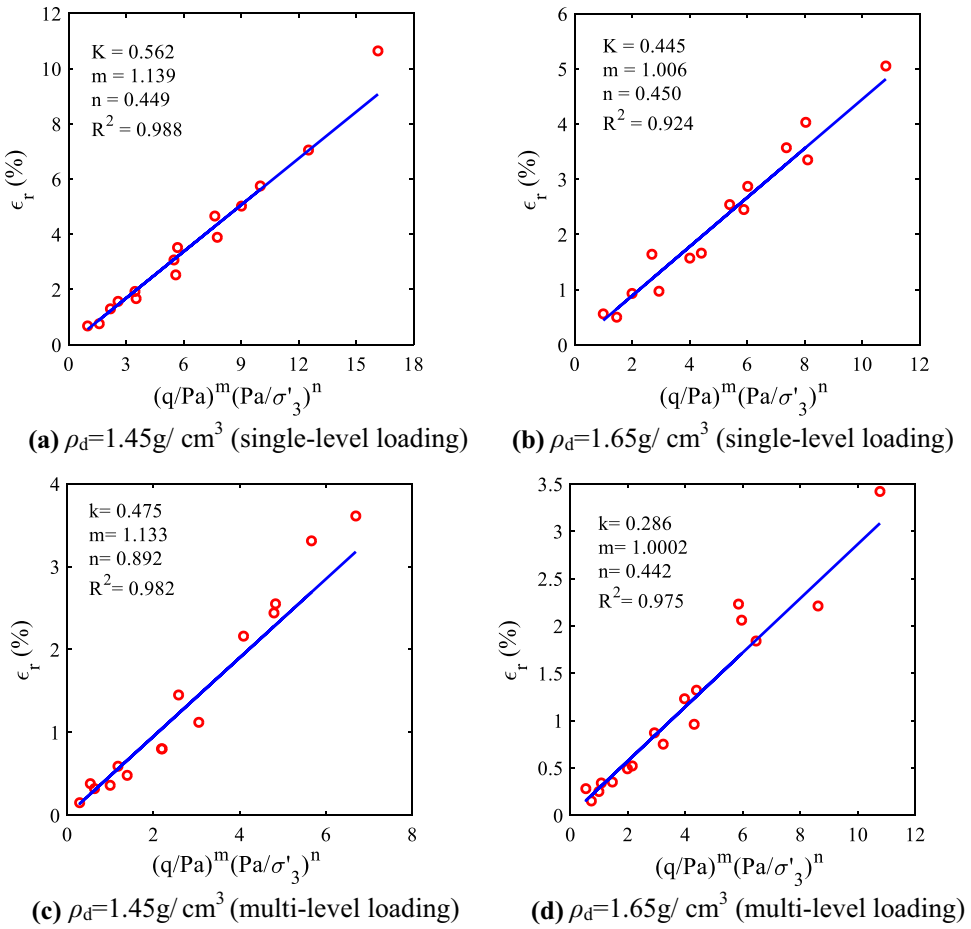

(a) ρ_d=1.45g/ cm^3 (single-level loading) **(b)** ρ_d=1.65g/ cm^3 (single-level loading)

(c) ρ_d=1.45g/ cm^3 (multi-level loading) **(d)** ρ_d=1.65g/ cm^3 (multi-level loading)

Fig. 16 Fitting relationship between elastoplastic strain ε_r in the loading phase and the stress conditions, described by $\frac{(q/P_a)^m}{(\sigma_3'/P_a)^n}$ of calcareous coral sand under different loading way

of the above Burgers soft-matter model, regained when $\beta = 1$, and $C = \eta_2$.

Compared with other empirical-based or element-based models, the Burgers soft-matter model could be widely applied in engineering practice, even though there are several more model parameters, and the calibration of these model parameters needs more work. Depending on the values of model parameters, the Burgers soft-matter model can describe different types of creep behavior of soil, for example, attenuated creep, steady creep, and accelerated creep when $0 < \beta < 1$, $\beta = 1$, and $\beta > 1$, respectively. The creep deformation predicted by the Burgers soft-matter model actually grows very slowly over time. It can be adopted to predict the long-term (could be decades) deformation of soil.

The creep deformation of sand is affected by its internal structure, stress condition, and time. The stress condition involves the effective confining pressure σ_3' and the deviatoric stress q.

A generalized equation can be constructed based on the above recognition:

$$\varepsilon_1 = f\left(\sigma_3', q, t\right) \tag{3}$$

Based on the analysis of the test data of the single-level and multi-level tests, we find that the initial elastoplastic deformation ε_r before the creep of the saturated calcareous coral sand is positively related to the applied q and inversely related to the σ_3'. Based on this recognition, the following equation is established:

$$\varepsilon_r = K\frac{(q/P_a)^m}{(\sigma_3'/P_a)^n} \tag{4}$$

where P_a=101.3 kPa is the atmospheric pressure used to formulate the equation with dimensionless variables. K, m, and n are dimensionless parameters.

The parameters K, m, and n can be determined by mathematically fitting the measured values of ε_r for the given values of σ_3' and q according to Eq. (4). It is found that the relationship between ε_r and $\frac{(q/P_a)^m}{(\sigma_3'/P_a)^n}$ is basically linear for the calcareous coral sand with different dry

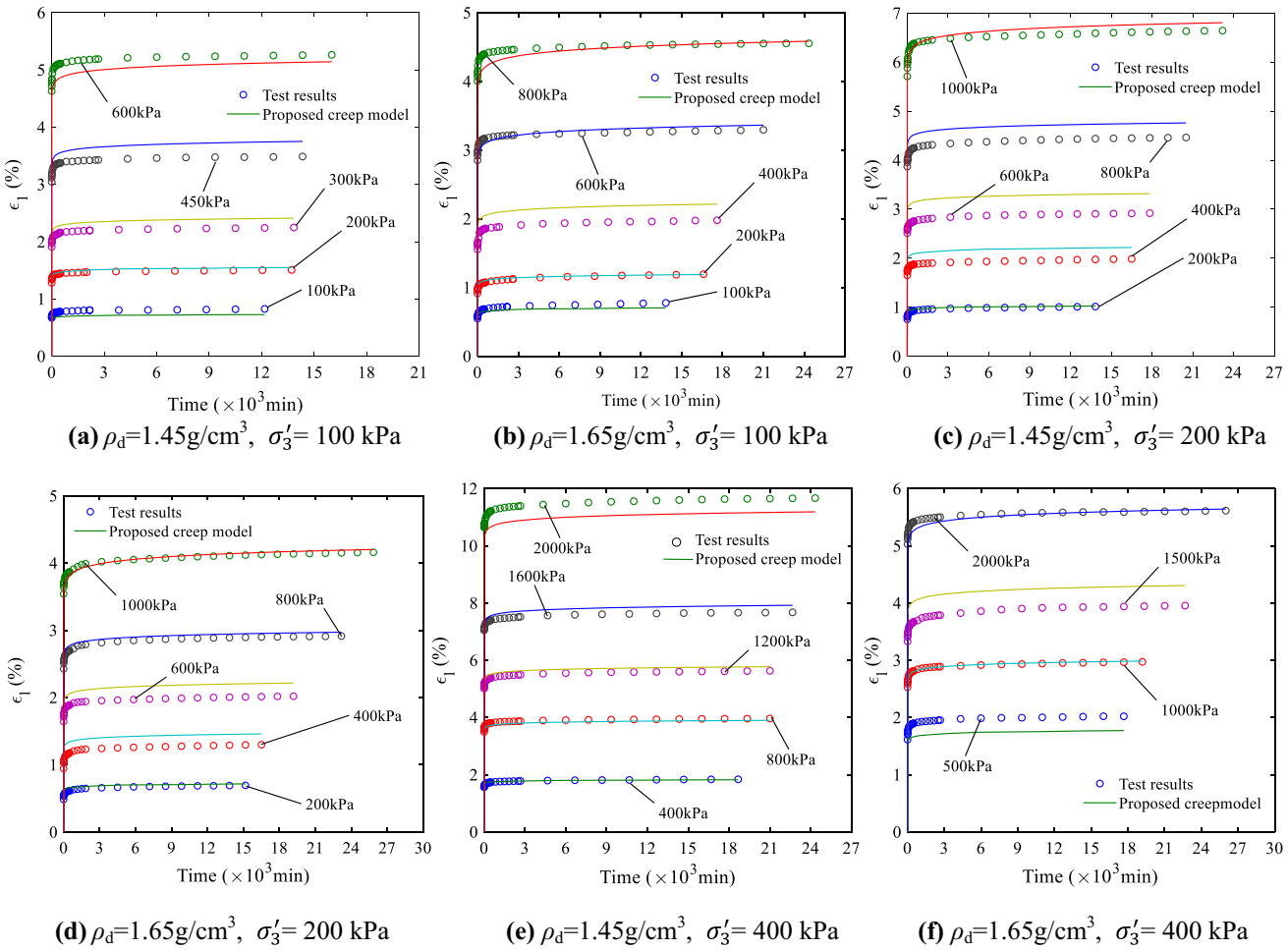

(a) ρ_d=1.45g/cm^3, σ_3'= 100 kPa **(b)** ρ_d=1.65g/cm^3, σ_3'= 100 kPa **(c)** ρ_d=1.45g/cm^3, σ_3'= 200 kPa

(d) ρ_d=1.65g/cm^3, σ_3'= 200 kPa **(e)** ρ_d=1.45g/cm^3, σ_3'= 400 kPa **(f)** ρ_d=1.65g/cm^3, σ_3'= 400 kPa

Fig. 17 Comparison between the creep test results and the predicted results by the modified creep model proposed in this study (single-level loading)

densities, as demonstrated in Fig. 16. It can be seen in Fig. 16 that the fitting degrees R^2 of each linear relationship are both greater than 0.92.

As mentioned above, the first item q/E_0in Eq. (1) actually represents the initial elastoplastic deformation, which is independent of time. E_0 is the initial deformation modulus of material. Combining Eq. (4) and the relationship $q = E_0\varepsilon_r$, the relationship between the initial deformation modulus E_0, $\sigma_3^{'}$, and q can be established as:

$$\frac{q}{\varepsilon_r} = E_0 = \frac{q}{K}\frac{\left(\sigma_3^{'}/P_a\right)^n}{\left(q/P_a\right)^m} \tag{5}$$

Substituting Eq. (5) into (1), the following modified Burgers soft-matter model is obtained:

$$\varepsilon_1 = K\frac{\left(q/P_a\right)^m}{\left(\sigma_3^{'}/P_a\right)^n} + \frac{q}{E_1}\left(1 - e^{-\frac{E_1}{\eta_1}t}\right) + \frac{q}{C}t^{\beta} \tag{6}$$

where the parameter K, m, and n under the conditions of single-level loading and multi-level loading have been successfully calibrated and listed in Fig. 16. By comparatively analyzing the values of the parameters K, m, and n under different loading conditions, as listed in Fig. 16, it is found that the value of n of medium dense coral sand under the condition of multi-level loading is greater than that under the condition of single-level loading. However, the values of n are basically the same under the two loading conditions for the dense coral sand. The variation of m is not significant under the two loading conditions, regardless of the dry density. The value of k is obviously related to the dry density of coral sand. Generally, the denser the sand is, the less the value of k is. Additionally, the value of k under the condition of multi-level loading is less than that under the condition of single-level loading; and this reduction of k is more obvious for the dense coral sand than the medium dense coral sand.

Meanwhile, the model parameters E_1, η_1, C, and β are also calibrated by adopting mathematical fitting for each creep curve. The calibrated E_1, η_1, C, and β are available in the Appendices 3 and Appendix 4. It should be noticed that a separate set of parameters (E_1, η_1, C, and β) is calibrated

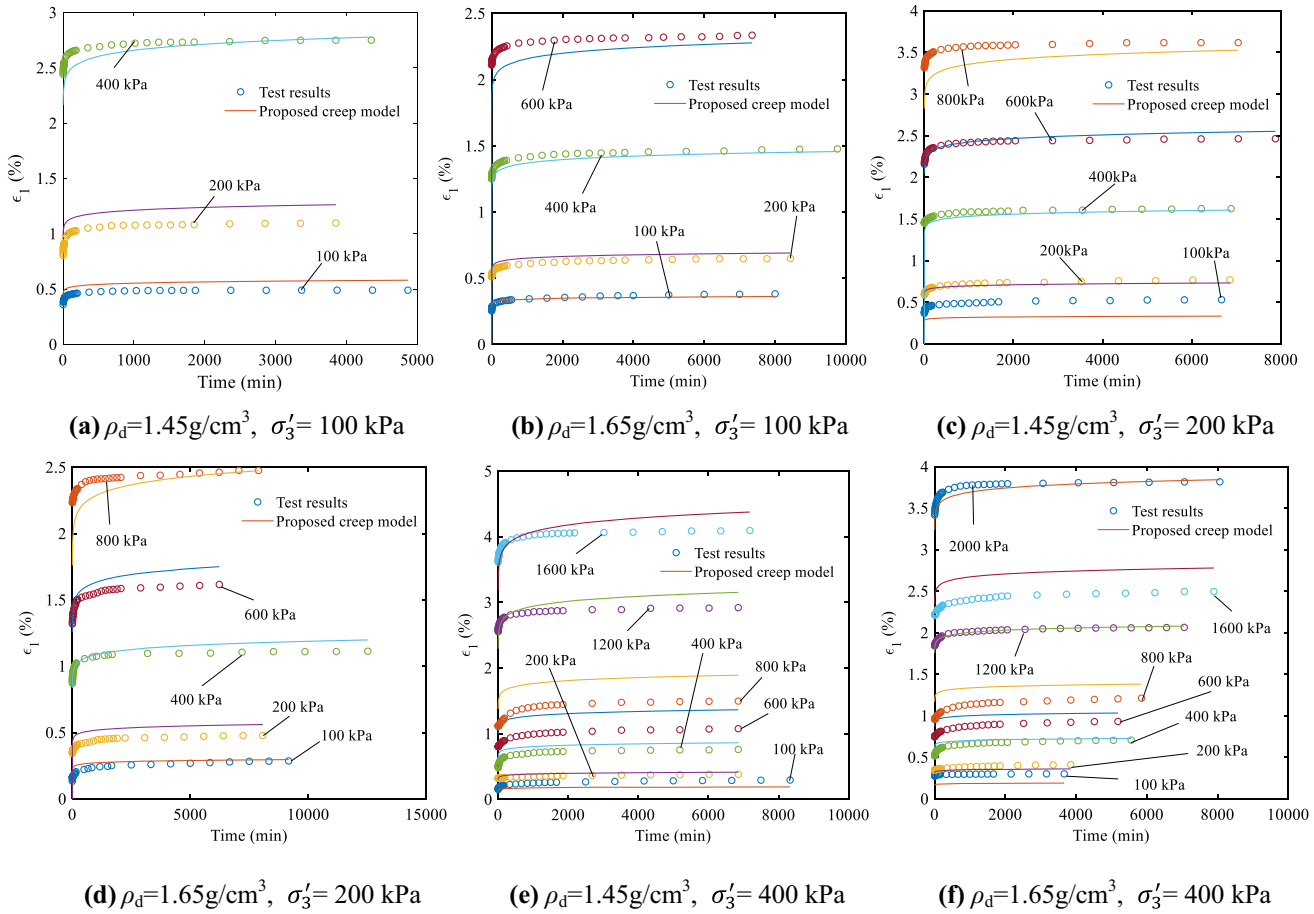

(a) ρ_d=1.45g/cm^3, σ_3'= 100 kPa **(b)** ρ_d=1.65g/cm^3, σ_3'= 100 kPa **(c)** ρ_d=1.45g/cm^3, σ_3'= 200 kPa

(d) ρ_d=1.65g/cm^3, σ_3'= 200 kPa **(e)** ρ_d=1.45g/cm^3, σ_3'= 400 kPa **(f)** ρ_d=1.65g/cm^3, σ_3'= 400 kPa

Fig. 18 Comparison between the creep test results and the predicted results by the modified creep model proposed in this study (multi-level loading)

for the creep curve under each level of deviatoric stress, regardless of the dry density, and the applied confining stress. Possible correlations between the model parameters E_1, η_1, C, and β and density, confining stress, and deviatoric stress were investigated, but no clear relationships could be found. This can be attributed to the scattering of test data and slight differences in the initial structure of the samples, while creep deformations are quite sensitive to this.

The comparison between the creep test results of coral sand under the condition of single-level loading and the predicted values by the modified Burgers soft-matter creep model is shown in Fig. 17. As illustrated in Fig. 17, it is found that the predicted deformations overall are in good agreement with the experimental results. However, there are also some biases for a few specimens, where the predicted creep curves are approximately parallel with the counterpart recorded in creep tests. It is indicated that the bias is mainly caused by the discrepancy in the initial elastoplastic deformation between the recorded values and the predicted values by Eq. (4) combining the fitting values of K, m, and n listed in Fig. 16.

The comparison between the creep test results of coral sand under the condition of multi-level loading and the predicted values by the modified Burgers soft-matter creep model is shown in Fig. 18 (Noted: the creep curve under each level of deviatoric stress is handled individually). As illustrated in Fig. 18, it is found that the modified soft-matter creep model can describe the creep curves of coral sand very well in some cases, e.g., q = 100 kPa and 200 kPa in Fig. 18b, q = 200 kPa, 400 kPa, and 600 kPa in Fig. 18c. In other cases, the predicted creep curves are approximately parallel with the measured counterparts due to the discrepancy between the test data and the predicted value by Eq. (4) for the initial elastoplastic deformation, e.g., q = 1600 kPa in Fig. 18f. However, the modified Burgers soft-matter creep model does not work very well for some creep curves, e.g., q = 1200 kPa and 1600 kPa in Fig. 18e. The main reason would be that when the model parameters E_1, η_1, C, and β for each creep curve are calibrated by adopting mathematical fitting according to Eq. (6), the initial elastoplastic deformation is firstly predicted by Eq. (4) using the calibrated parameters K, m, and n listed in Fig. 16. This predicted initial elastoplastic

deformation with discrepancy then will be taken into consideration when calibrating the model parameters E_1, η_1, C, and β for each creep curve in this study. As a result, the predicted initial elastoplastic deformation with discrepancy must have an unfavorable effect on the calibration of the parameters E_1, η_1, C, and β. If the above-mentioned unfavorable effect is not considered, then the predicted creep curves must be parallel or overlapped with the experimental creep curves. Overall, the suitability of the modified Burgers soft-matter creep model is acceptable.

Generally speaking, compared with the Mesri model and the original Burgers model, there are fewer parameters that need to be calibrated in the modified Burgers soft-matter creep model proposed in this study. It could greatly reduce the workload in the process of parameter calibration. The comparative illustration for the Mesri, original Burgers, and modified Burgers soft-matter models for the calcareous coral sand from SCS is available in Cao [3] and Haiyilati [7]. Overall, the reliability of this proposed modified model is acceptable, as analyzed above. Finally, it is worthy to notice that the deformation predicted by this modified creep model does not converge with time. It can be used to predict the extremely long-term post-construction subsidence of structures induced by the creep behavior of foundation.

5 Conclusion

In this study, a series of CD triaxial creep tests under different loading ways (single-level and multi-level) are conducted to study the creep characteristics of calcareous coral sand sampled from a natural coral reef in the South China Sea (SCS). A modified creep model for the calcareous coral sand is proposed based on the experimental results. This study mainly has the following conclusions:

(1) When the applied q is less than the failure strength q_f, attenuated creep is generated in the saturated calcareous coral sand under various stress conditions. The final creep deformation of calcareous coral sand accounts for about 8–30% of the total deformation, which is of considerable magnitude. Under the condition of multi-level loading, if $\sigma_3^{'}$ is high and the applied q is close to the failure strength q_f, calcareous coral sand will present the "time lag effect of creep deformation." Moreover, the shear failure of calcareous coral sand also presents the "time lag effect of failure" when the applied q reaches the failure strength. However, the two types of time lag effects are not observed under the condition of single-level loading.

(2) It is found that there are two development modes for the $\varepsilon_v - \varepsilon_1$ curves during creeping under single-level loading for the calcareous coral sand. The first one is that there is only contraction during creeping if the axial strain ε_1 at the end of the initial loading stage (corresponding to the vertical dotted line in Fig. 8) is not significantly larger than the ε_1 at phase transformation point. Otherwise, there is only continuous dilation during creeping. Unfortunately, the quantitative description for the above statement "not significantly more than" cannot be given so far. Under the condition of multi-level loading, there is only contraction observed during creeping.

(3) Due to the existence of micro inner cavities and the effect of surface tension of pore water, some air inevitably is trapped in these micro inner cavities during the specimen saturation. Due to a time-dependent compression of these air inclusions under constant back pressure, a spurious dilative ε_v was measured by a piston-type volumetric controller in the middle and late stages of creep in some of the tests, i.e., the measured creep response changes from contractive to dilative. Based on this recognition, it is recommended to measure the volumetric strain during the creeping of calcareous coral sand by adopting other methods, rather than a piston-type volumetric controller. There are also several specimens for which the transformation from contractive to dilative response is not observed during the whole creeping, even though their sand particles also contain micro inner cavities. Currently, the reason for this observed phenomenon cannot be explained so far and needs more comprehensive research works in the future.

(4) It is found that the $\varepsilon_v - \varepsilon_1$ curves during creeping are generally not consistent with those recorded in monotonic tests. Therefore, the potential surface for elastoplastic strain cannot be copied when developing a visco-elastoplastic constitutive soil model for calcareous coral sand.

(5) Although some particle breakage has occurred in the creep process, the amount of particle breakage is very low for the calcareous coral sand from the SCS. Therefore, it can be concluded that the sliding and rearrangement of particles play a dominant role in the creep deformation process, while the contribution of particle breakage is minor.

(6) It is demonstrated that the modified soft-matter model proposed in this study is acceptable to describe the creep behavior of the calcareous coral sand from the SCS. It could be a solid basis for the subsequent development of a visco-elastic–plastic constitutive model for calcareous coral sand. It also

could be applied for predicting the long-term post-construction settlement of some large structures built on reclaimed coral sand foundations, such as the airports and ocean lighthouses in the SCS, in the next 10, 20, and 50 years [47, 46].

Appendix 1: Proportion of creep strain of the calcareous coral sand when creep tests are finished (single-level loading)

Dry density (g/cm^3)	σ_3'(kPa)	q (kPa)	ε_0(%)	ε_c(%)	$\varepsilon_{\text{Total}}$(%)	Creep strain percentage (%)
1.45	100	100	0.67	0.16	0.83	19
		200	1.28	0.23	1.51	15
		300	1.91	0.34	2.25	15
		450	3.04	0.45	3.49	13
		600	4.63	0.63	5.26	12
	200	200	0.75	0.26	1.01	26
		400	1.65	0.34	1.99	17
		600	2.51	0.41	2.92	14
		800	3.87	0.59	4.46	13
		1000	5.71	0.93	6.64	14
	400	400	1.56	0.28	1.84	15
		800	3.49	0.47	3.96	12
		1200	5.01	0.62	5.63	11
		1600	7.04	0.63	7.67	8
		2000	10.64	1.03	11.67	9
1.65	100	100	0.55	0.23	0.78	29
		200	0.92	0.27	1.19	20
		400	1.56	0.42	1.98	21
		600	2.85	0.44	3.29	13
		800	4.01	0.54	4.55	12
	200	200	0.48	0.21	0.69	30
		400	0.94	0.36	1.30	28
		600	1.64	0.38	2.02	19
		800	2.43	0.48	2.91	16
		1000	3.54	0.62	4.16	15
	400	500	1.61	0.41	2.02	20
		1000	2.53	0.44	2.97	15
		1500	3.33	0.63	3.96	16
		2000	5.03	0.59	5.62	10

Appendix 2: Proportion of creep strain of the calcareous coral sand when creep tests are finished (multiple-level loading)

Dry density (g/cm^3)	σ_3'(kPa)	q (kPa)	ε_0(%)	ε_c(%)	ε_{Total} (%)	Creep strain percentage (%)
1.45	100	100	0.34	0.15	0.49	31
		200	0.28	0.33	0.61	54
		400	1.31	0.34	1.65	21
	200	100	0.36	0.17	0.53	32
		200	0.05	0.18	0.23	78
		400	0.57	0.29	0.86	34
		600	0.52	0.33	0.85	39
		800	0.64	0.51	1.15	44
	400	100	0.15	0.15	0.30	50
		200	0.02	0.07	0.09	77
		400	0.08	0.30	0.38	79
		600	0.03	0.28	0.31	90
		800	0.03	0.39	0.42	93
		1200	0.84	0.58	1.42	41
		1600	0.03	1.14	1.17	97
1.65	100	100	0.23	0.15	0.38	39
		200	0.09	0.18	0.27	67
		400	0.47	0.35	0.82	43
		600	0.40	0.44	0.88	50
	200	100	0.13	0.15	0.28	54
		200	0.06	0.13	0.19	68
		400	0.38	0.26	0.64	41
		600	0.12	0.36	0.48	75
		800	0.45	0.43	0.88	49
	400	100	0.28	0.02	0.30	7
		200	0.04	0.07	0.11	64
		400	0.06	0.24	0.30	80
		600	0.03	0.18	0.22	82
		800	0.03	0.25	0.28	89
		1200	0.36	0.47	0.83	57
		1600	0.15	0.31	0.46	67
		2000	≈ 0	1.31	1.31	100

Appendix 3: Model parameters of modified Burgers soft-matter model for the calcareous coral sand (single-level loading)

Dry density (g/cm^3)	σ_3'(kPa)	q (kPa)	E_1 (MPa)	η_1	C	β
1.45	100	100	1.733	60.146	16.815	0.289
		200	2.326	65.803	19.94	0.265
		300	2.686	61.955	14.164	0.245
		450	2.563	71.622	15.674	0.229
		600	2.016	52.286	19.900	0.247
	200	200	2.543	202.146	9.103	0.220
		400	4.482	167.052	18.002	0.239
		600	5.430	529.240	25.136	0.255
		800	4.164	321.049	22.995	0.244
		1000	2.773	121.516	18.041	0.227
	400	400	5.568	217.076	10.091	0.184
		800	6.289	184.971	10.016	0.159
		1200	8.392	287.890	13.156	0.185
		1600	11.188	658.118	20.592	0.200
		2000	4.777	653.488	46.264	0.272
1.65	100	100	2.134	159.731	2.717	0.176
		200	4.346	80.288	5.281	0.196
		400	2.553	232.302	6.167	0.156
		600	3.844	107.735	9.096	0.161
		800	3.874	126.230	9.851	0.160
	200	200	4.404	252.107	12.330	0.232
		400	4.319	318.055	12.508	0.208
		600	4.580	247.576	26.110	0.234
		800	7.105	852.303	19.995	0.219
		1000	7.396	572.481	24.963	0.242
	400	500	4.029	124.352	7.705	0.166
		1000	7.007	304.348	18.245	0.190
		1500	12.397	488.071	17.951	0.195
		2000	10.096	420.667	23.579	0.167

Appendix 4: Model parameters of modified Burgers soft-matter model for the calcareous coral sand (multiple-level loading)

Dry density (g/cm^3)	σ_3'(kPa)	q (kPa)	E_1 (MPa)	η_1	C	β
1.45	100	100	168.321	3893	393	0.150
		200	147.710	3731	368	0.159
		400	295.639	6264	1018	0.208
	200	100	187.652	5000	826	0.263
		200	318.319	26637	1953	0.285
		400	492.61	93050	5884	0.302
		600	336.13	25406	12292	0.364
		800	457.4	40839	17123	0.377
	400	100	328.41	31366	690	0.237
		400	308.64	22594	3110	0.289
		600	455.93	126190	12074	0.389
		800	287.05	105726	39138	0.466
		1200	630.25	22309	46012	0.496
		1600	507.94	51493	136286	0.552
1.65	100	100	309.21	5203	597	0.214
		200	540.102	44270	1648	0.247
		400	507.87	50484	2900	0.260
		600	720.89	83417	4207	0.262
	200	100	392.16	104269	523	0.208
		200	410.26	107368	1785	0.235
		400	3584	7977	2487	0.247
		600	456.62	42875	3322	0.263
		800	785	155770	7207	0.289
	400	100	807.7	18620	6134	0.267
		400	585.9	60025	3108	0.275
		600	859.9	236905	11871	0.373
		800	676.2	188527	20613	0.412
		1200	939.7	146052	55710	0.431
		1600	1124.4	247389	85607	0.492
		2000	685.87	73813	267594	0.544

Acknowledgements We sincerely appreciate the financial support from the National Natural Science Foundation of China under Project No. 51879257.

Funding National Natural Science Foundation of China under Project No. 51879257.

data availability Depending on the request from the corresponding author.

Declarations

Conflict of interest There is no conflict of interest.

References

1. Andò E, Dijkstra J, Roubin E, Dano C, Boller E (2019) A peek into the origin of creep in sand. Granular Matter 21:11
2. Brzesowsky RH, Hangx SJT, Brantut N et al (2014) Compaction creep of sands due to time-dependent grain failure: effects of chemical environment, applied stress, and grain size. J Geophys Res: Solid Earth 119:7521–7541
3. Cao M (2019) Research on creep characteristics of calcareous sand in the South China Sea. Master thesis, Wuhan University of Technology, China
4. Chen B, Chao DJ, Wu WJ, Hu JM (2019) Study on creep mechanism of coral sand based on particle breakage evolution law. J Vibroeng 4(21):1201–1214
5. Firme PALP, Brandao NB, Roehl D et al (2018) Enhanced double-mechanism creep laws for salt rocks. Acta Geotech 13:1329–1340
6. Gao R, Ye JH (2019) Experimental investigation on the dynamic characteristics of calcareous sand from the reclaimed coral reef islands in the South China Sea. Rock Soil Mech 40(10):3897–3908
7. Haiyilati Y (2021) Experimental study on the creep characteristics of the reclaimed calcareous coral sand in the South China Sea. Master thesis, Wuhan University of Technology, China
8. Han J, Yin Z, Dano C et al (2020) Cyclic and creep combination effects on the long-term undrained behavior of overconsolidated clay. Acta Geotech
9. He LJ, Kong LW, Wu WJ et al (2011) A description of creep model for soft soil with fractional derivative. Rock Soil Mech 32(2):239–244
10. Karimpour H, Lade PV (2013) Creep behavior in Virginia Beach sand. Can Geotech J 50:1159–1178
11. Kondner RL (1963) Hyperbolic stress-strain response: cohesive soils. J Soil Mech 89(1):115–143
12. Lade PV, Liu CT (1998) Experimental study of drained creep behavior of sand. J Eng Mech 124(8):912–920
13. Lade PVL, Liu CT (1998) Experimental study of drained creep behavior of sand. J Eng Mech 124(8):15570
14. Lade PV, Nam J, Liggio CD Jr (2010) Effects of particle crushing in stress drop-relaxation experiments on crushed coral sand. J Geotech Geoenviron Eng 136(3):500–509
15. Li J, Tang Y, Feng W (2020) Creep behavior of soft clay subjected to artificial freeze–thaw from multiple-scale perspectives. Acta Geotech 15:2849–2864
16. Liu CQ, Wang R (1999) Evaluation of calcareous sand grains crushing and its energy equation. J Eng Geol 7(4):366–371
17. Liu S, Wang JF, Kork CY (2019) DEM simulation of creep in one-dimensional compression of crushable sand. J Geotechn Geoenviron Eng 145(10):04019060
18. Liu HB, Zeng KF, Zou YZ (2020) Particle breakage of calcareous sand and its correlation with input energy. Int J Geomech 20(2):04019151
19. Lv YR, Li F, Liu YW, Wang MY (2017) Comparative study of coral sand and silica sand in creep under general stress states. Can Geotech J 54(11):1601–1611
20. Maqsood Z, Koseki J, Miyashita Y, Xie JR, Kyokawa H (2020) Experimental study on the mechanical behaviour of bounded geomaterials under creep and cyclic loading considering effects of instantaneous strain rates. Eng Geol 276:105774
21. Markovitz H (1977) Boltzmann and the beginnings of linear viscoelasticity. Trans Soc Rheol 21:381
22. Mesri G, Febres-Cordero E, Shields DR, Castro A (1981) Shear stress-strain-time behavior of clays. Geotechnique 31(4):537–552
23. Murayama S (1983) Formulation of stress-stain-time behavior of soils under deviatoric stress condition. Soils Found 23(2):43–57
24. Murayama S, Michihiro K, Sakagami T (1984) Creep characteristics of sands. Soils Found 24(2):1–15
25. Nishihara M (1958) Rheological properties of rocks I and II. Doshisha Engineering Review, 8:32–5 and 85–115
26. Obituary (1982) Jan Burgers. Physics Today. 35(1): 84–85. January
27. Peng Y, Ding XM, Xiao Y et al (2019) Study of particle breakage behavior of calcareous sand dyeing tracking and particle image segmentation method. Rock Soil Mech 40(7):2663–2672
28. Riaz B, Juan R, Tommy E (2015) Evaluation of primary and secondary deformations and particle breakage of tailings. Fund Appl Geotech 119:2481–2488
29. Singh A, Mitchell JK (1968) General stress-strain-time function for soils. J Soil Mech Found Div 94(1):24–46
30. Sun Y, Chen C (2018) Fractional order creep model for coral sand. Mech Time-Dep Mater 8:1–12
31. Sun JZ, Wang R (2003) Study on particle failure process of calcareous sand under triaxial compression. Rock Soil Mech 24(5):822–825
32. Tong CX, Burton G, Zhang S, Sheng DC (2020) Particle breakage of uniformly graded carbonate sands in dry/wet condition subjected to compression/shear tests. Acta Geotech 15(5):1–14
33. Wang YF, Cai YY, Cai ZY (2017) Experimental investigation of creep properties of saturated sand. J Huaqiao Univ (Natural Science) 38(1):31–37
34. Wang YQ, Hong Y, Guo Z, Wang LZ (2018) Micro-and macro mechanical behavior of crushable calcareous sand in South China Sea. Rock Soil Mech 39(1):199–207
35. Wang YS, Ma LJ, Wang MY, Lv YR, Dong L, Fan PX (2018) A creep constitutive model incorporating deformation mechanisms for crushable calcareous sand. Arab J Geosci 11:623–630
36. Wang XZ, Wang X, Weng YL, Lv SZ, Yan K, Zhu CQ (2016) Characteristics of dry density of calcareous sand and its testing methods. Rock Soil Mech 37(2):316–322
37. Wang S, Wang JG, Wu W, Cui DS, Su AJ, Xiang W (2020) Creep properties of clastic soil in a reactivated slow-moving landslide in the Three Gorges Reservoir Region, China. Eng Geol 267:105493
38. Wang G, Wang ZN, Zha JJ (2020) Particle breakage evolution of coral sand using triaxial compression tests. J Rock Mech Geotech Eng 13(3):321–334
39. Wen Z, Duan ZG, Li SD et al (2019) Shear mechanical properties of dredged coral sand from the South China Sea. J Eng Geol
40. Xie X, Qi SW, Zhao F, Wang DH (2018) Creep behavior and the microstructural evolution of loess-like soil from Xi'an area, China. Eng Geol 236(26):43–59
41. Xu M, Jin D, Song E et al (2018) A rheological model to simulate the shear creep behavior of rockfills considering the influence of stress states. Acta Geotech 13:1313–1327
42. Yang Q, Leng MW, Nie RS, Zhou W, Zhu W (2014) Laboratory test study of creep behavior of sandy. Chin J Rock Mech Eng 33(S2):4282–4286
43. Ye JH, Cao M, Gang Li (2019) Preliminary study on the creep characteristics of calcareous sand from reclaimed coral reef islands in South China Sea. Chin J Rock Mech Eng 38:1242–1251
44. Yin DS, Ren J, He CL et al (2007) A new rheological model element for geomaterials. Chin J Rock Mech Eng 26(9):1899–1903

45. Yu HZ, Wang R (1999) The cyclic strength test research on calcareous sand. Rock Soil Mech 20(4):6–11
46. Yu DW, Ye JH (2021) Numerical modelling of the creep subsidence of an ocean lighthouse constructed on a reclaimed Coral Reef Island. KSCE J Civ Eng 25(4):1191–1203
47. Yu DW, Ye JH, Yao LH (2020) Prediction of the long-term settlement of the structures built on a reclaimed coral reef island: an aircraft runway. Bull Eng Geol Env 79(9):4549–4564
48. Zhang JM, Zhang L, Liu H et al (2008) Experimental research on shear behavior of calcareous sand. Chin J Rock Mech Eng 27(S1):3010–3015
49. Zhao J, Feng XT, Zhang XW, Yang CX (2019) Brittle and ductile creep behavior of Jinping marble under true triaxial stress. Eng Geol 258:105157
50. Zhao ZY, Qiu YY, Zi M et al (2019) Experimental study on dynamic compression of unsaturated calcareous sand. Explosion Shock Waves 40(2):023102
51. Zhu CQ, Chen HY, Meng QS, Wang R (2014) Microscopic characterization intra-pore structures of calcareous sands. Rock Soil Mech 35(7):1831–1836
52. Zuo RF, Du GX, Yang WG, Liao LB, Li ZH (2016) Mineralogical and chemical characteristics of a powder and purified quartz from Yunnan Province. Open Geosci 8(1):606–611

Publisher's Note Springer Nature remains neutral with regard to jurisdictional claims in published maps and institutional affiliations.